A general strategy for performance enhancement of negative stiffness mechanical metamaterials

Xiaojun Tan[a, b], Kaili Yao[a], Shaowei Zhu[c], Bing Wang[a*], Muamer Kadic[b]

[a] National Key Laboratory of Science and Technology on Advanced Composites in Special Environment, Harbin Institute of Technology, Harbin 150080, P.R. China

[b] Institute FEMTO-ST, CNRS, University Bourgogne Franche-Comté, 25000 Besançon, France

[c] College of Aerospace Engineering, Chongqing University, Chongqing, 400030, China

Abstract: Negative stiffness mechanical metamaterial possesses many interesting properties such as high energy absorption and dissipation efficiency but fairly low strength. Introducing filling material appears to be a very effective strategy to enhance the cellular materials' mechanical properties. In this work, we show how to improve the basic mechanical properties, energy dissipation and absorption capacity of the cylindrical negative stiffness structure via introducing filling materials. We first offer the principle of the negative stiffness material combined with an alternative mechanism and then we further investigate the mechanical response of the filler-free structure and the filled structure with different filling materials (linear elastic, visco-hyperelastic, and true negative stiffness). We demonstrate that the linear elastic filler can improve the energy absorption property but degrade the energy dissipation performance. The visco-hyperelastic filler can enhance the energy dissipation capacity of the structure whether the snap-back behavior exists or not. The true negative stiffness filler can improve the structure's energy dissipation capacity and decrease the strength simultaneously. The

*Corresponding author; Tel.:+86 451 86402376; fax: +86 451 86402386
E-mail address: wangbing86@hit.edu.cn (Bing Wang)

presented methods can be seen as a reference to the design of other negative stiffness mechanical metamaterials.

Keywords: negative stiffness, mechanical metamaterials, visco-hyperelastic filler, energy dissipation capacity, performance enhancement

1. Introduction

Conventional natural and artificial materials usually exhibit an increasing load as the deformation proceeds before yield or buckling, while the negative stiffness (NS) mechanical metamaterials are characterized by an increase in deformation resulting in a load drop within a specific strain range. NS mechanical metamaterials are constructed with periodically arranged NS element, and possess many exciting properties, such as multi-stable and snap-back behaviors. Harnessing the multi-stable property, the NS mechanical metamaterials can be applied to tune the propagation of various types of waves, like force[1-3], sound[4], and light[5,6]. NS mechanical metamaterials, on the other hand, show a long stress plateau owing to the snap-back behavior and therefore are promising in impact protection and isolation.

Research into NS behavior has a long history. For many years, most research in this field mainly focused on the NS elements and mechanism, such as the spring system[7], beam element[8,9], shell element[10-14], origami[15,16], and magnets system[17]. This mechanical behavior was only used in constructing quasi-zero stiffness vibration isolation system[9,18-20] and designing some micro-electro-mechanical system[21-23] (e.g.,

relays and valves). Over the past two decades, researchers attempted to apply the NS mechanism to advanced damper[24-26], advanced actuators[27,28], energy harvesting devices[29], and deployable structures[30].

Prasad et al.[31] first designed a periodic cellular structure by arranging the NS beam elements, and this structure is an embryonic form of the NS mechanical metamaterials. According to the current definition, the NS mechanical metamaterial is constructed by arranging the elements with NS property along particular directions and can exhibit periodic snap-through behavior and NS response. Although the design concept of the NS mechanical metamaterials was presented early, its great potential received too little attention at that time.

In 2010, Feeny et al.[32] demonstrated that an oscillatory behavior could be observed in a chain of masses connected by nonlinear springs under quasi-static loading. The oscillatory behavior is exactly the primary energy dissipation mechanism of the current NS mechanical metamaterials, and it is only since this work that the study of NS behavior has gained new momentum. The oscillatory behavior in the NS mechanical metamaterials has been extensively studied[33-38] and came to be known as a snap-back behavior in some literatures[39]. The NS mechanical metamaterials with the snap-back behavior can exhibit long, time-independent stress plateau and possess high and tailorable energy dissipation capacity. Harnessing the snap-back behavior, various types of NS mechanical metamaterials[40-52] were designed and studied. In addition, the possible applications of the NS mechanical metamaterial in other fields, like deployable structures[53-58], tuning waves[3,59-62], and impact isolation[42,63-68], have also been widely

explored.

Though the NS mechanical metamaterials have several advantages, such as the high energy dissipation efficiency, fully reversible, and rate-independent properties over traditional energy absorption materials, they typically exhibit relatively low strength and specific energy absorption[69]. A considerable amount of literature on the enhancement of the NS mechanical metamaterials' properties has been published to address this issue. These studies can be broadly divided into three categories: novel mechanisms[46,70,71] to realize NS behavior, introducing viscoelasticity materials[68,72], and structural topology optimization[73]. Novel NS mechanical metamaterials, such as the multi-stable shape-reconfigurable architected materials[46], and the bio-inspired multi-stable metamaterials[74], did improve the strength and specific energy dissipation capacity by several orders of magnitude. However, proposing new mechanisms relies much on inspiration and is frequently haphazard. The strategy, topology optimization[31,73], has been extensively studied and widely used to improve the architected cellular materials. Introducing filling materials, also as a general performance enhancement strategy for architected cellular materials, by contrast, has received scant attention in the research of this field.

In this study, the mechanical properties of a cylindrical NS structure are attempted to be improved via introducing filling materials. We first discuss the central concept of how an additional filling material can improve/change the mechanical properties. Then, the influence of the filling material type on the filled NS structure is systematically investigated through a combination of analytical, numerical, and experimental methods.

Finally, conclusions are drawn, and references are listed at the end of the paper.

2. Basic principle of filled NS structures

It is essential to notice that, in general, adding a microstructure into a host material and computing its properties is a challenging task[75]. In this paper, we consider a straightforward case to start: a uniaxial NS element depicted in Fig. 1(a). In the middle of column one, we can see that the stress-stain curve is manly characterized by the peak and the valley point. As shown in the bottom of column one, it is only once such structures are placed in serial that one will see a net energy dissipation via phonon dissipation mechanism (snap-back), mainly given by the hysterical curve of loading and unloading of the structure. Moreover, the plateau stress in loading and unloading processes respectively is equal to that of the single element's peak and valley response points.

Assuming that the curve was optimized in a way that the overall behavior should be repeatable without destroying the metamaterial, we ask ourselves how to still improve the energy absorption by adding filler.

Schematically, from columns 2-4, we depict three ways to add in an additional parallel spring to the NS. It turns out to be a relatively simple calculation in the first place. However, the result is rather striking and is depicted in Fig 1(c).

We note that if add a spring in parallel, the force response is increased, as shown in the middle of column 2. In the opposite case, if we add a negative-like spring, the overall curve's minimum is decreased, as depicted in the middle of column 4.

The critical aspect is that the enclosed area of the hysteresis for the NS structure

(NS element in series) with negative-like springs expands significantly, as shown in the bottom of column 4. In contrast, that area for the NS structure with simple springs shrinks, as shown in the bottom of column 2. The key mechanism for the above phenomena is that the negative-like spring would widen the gap between the maximum and the minimum response point, as shown in the middle of column 4, while a simple spring would narrow that gap, which directly determined the plumpness of the hysteresis.

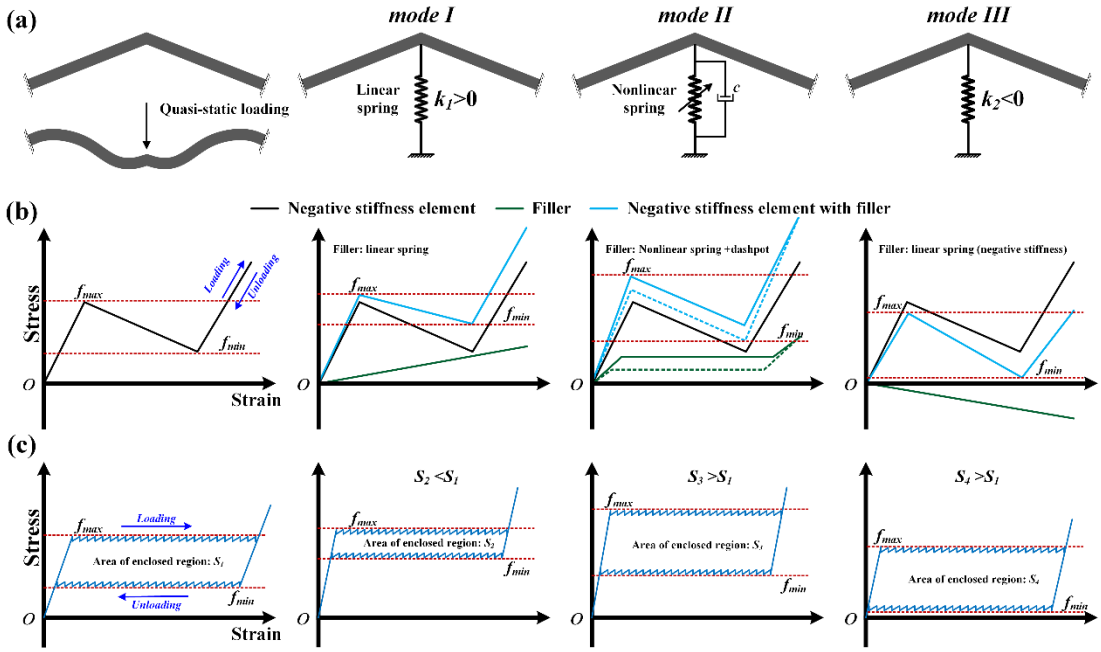

Fig. 1. Principles of parallel coupling of NS element with other different springs. (a) Mechanical system is depicted: NS element; NS element filled with a single spring; NS element filled with a nonlinear spring coupled with dashpot; NS element filled with a negative-like spring; (b) behavior of NS element and each different spring, and combination of both; (c) behavior of such combined elements when arranged in series and the energy absorption area. Column one: NS alone. Column two: NS element with a simple spring. Column three: NS element integrated with nonlinear spring coupled with dashpot. Column four: NS element with a negative-like spring.

The core of this study is to exploit the filler to tune the difference between the maximum and the minimum response point of the NS element and improve the properties of the NS structures. Although the visco-hyperelastic filler can also enhance the energy dissipation capacity of the NS structure, as shown in column 3, the main role of the filler here is to tune the response of the NS element rather than to absorb energy directly. The visco-hyperelastic filler, described by a nonlinear spring coupled with a dashpot, possesses a long stress plateau, and an obvious hysteresis loop, as shown in the middle of column 3. Thus, it can increase the maximum and minimum response simultaneously and widen their gap. The visco-hyperelastic material is a frequently used filler in the lattice structures, but its mechanism is entirely different in this study.

3. Investigated metamaterial and its substructure

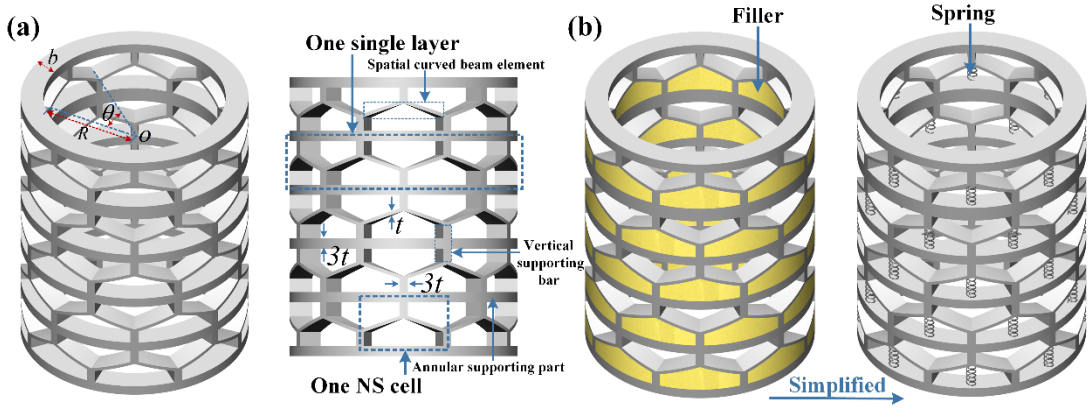

Fig. 2. (a) Diagram of cylindrical NS structure, isometric view and front view; (b) cylindrical NS structure with filler in cell elements and its simplified form.

The research object in this study is a cylindrical NS structure, and its structure diagrams are displayed in Fig. 2(a) and (b). The NS property and the basic mechanical properties of the cylindrical NS structure have been studied in our previous work[65,76], which suggested that the structure's mechanical response are mainly determined by the

following structural parameters: h, the apex height of the spatial inclined beam element, t, the thickness of the spatial inclined beam element, b, the width of the spatial inclined beam element, R, the inside radius of the cylindrical structure, A, the number of the cell in one layer, and n, the number of the structure's layer. The vertical supporting bars and the annular supporting parts may weaken the NS property if these parts are not strong enough. To prevent the negative influence, the thickness of the vertical bar and the annular part are both set as three times that of the spatial inclined beam element, i.e., $3t$, as shown in Fig. 2(a). The diagrams of the filled cylindrical NS structures are displayed in Fig. 2(b), and the filler in each element can be the linear elastic, the visco-hyperelastic, and the true negative stiffness materials.

Tab. 1. Structural parameter values of cylindrical NS structure's sample

Apex height, h (mm)	6	Inside radius, R (mm)	40
Thickness, t (mm)	1.5	Number of cells in one layer, A	7
Width, b (mm)	10	Number of the layer, n	8

Samples of the unfilled and the filled cylindrical NS structures were fabricated for testing and comparative study. The physical picture of the cylindrical NS structure is displayed in Fig. 3(a), and its structural parameter values are listed in Tab. 1. This sample was fabricated with the gel-casting method, and the detailed fabrication process can be found in our previous research[76]. The physical pictures of the filled cylindrical NS structures with the polyurethane sponge (visco-hyperelastic) are shown in Fig. 3(b). The physical picture of the selected polyurethane sponge with different densities is shown in Fig. 3(d).

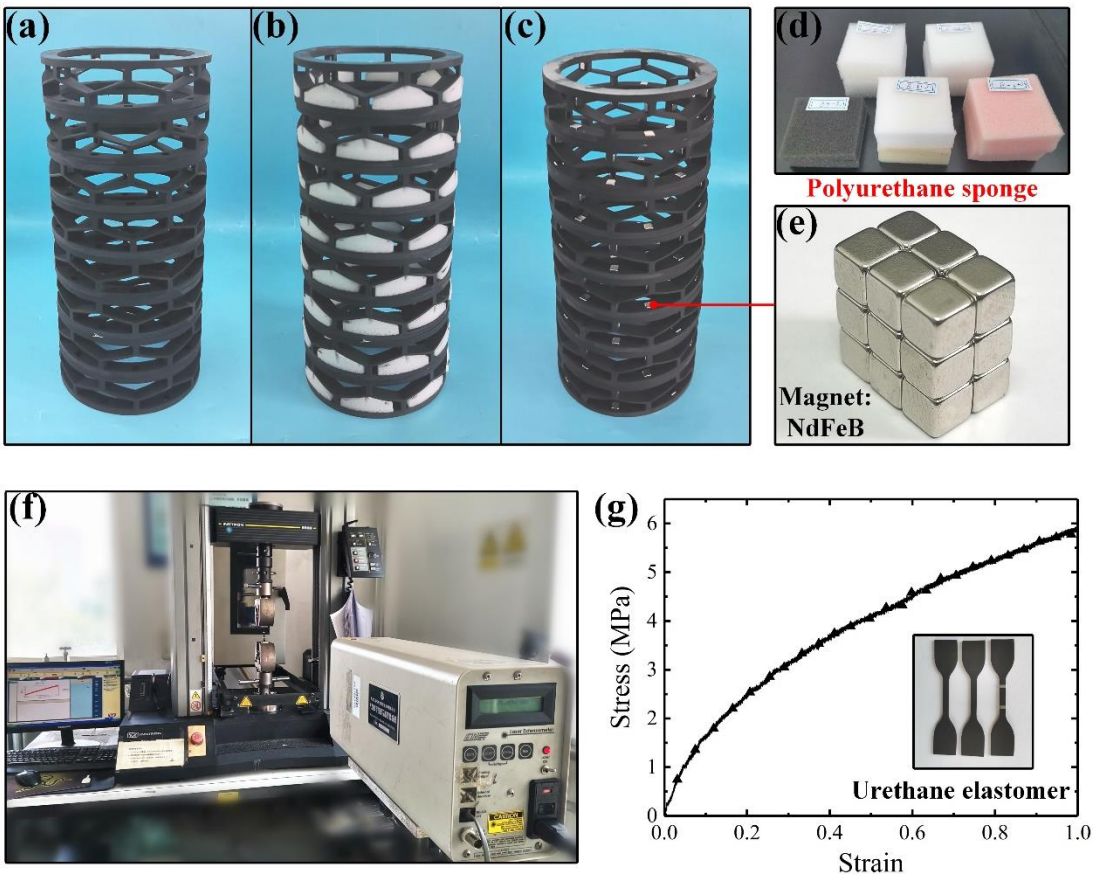

Fig. 3. (a) Physical picture of unfilled cylindrical NS structure. Physical picture of filled cylindrical NS structure with (b) polyurethane sponge; (c) magnets systems. (d) Visco-hyperelastic filler, polyurethane sponge; (e) physical pictures of selected magnets; (f) experiment setups for standard tensile tests and experiment equipment for loading-unloading test (INSTRON 5569); (g) true stress-strain response curve of structure's base material and dog-bone-shaped specimens.

These sponges for filling were purchased from the supplier (New Jiayuan Industrial & Trading, China) and were cut into particular shapes through the punching process for filling. In Fig. 3(c), magnets are embedded in the cylindrical NS structure and act as the true NS filler. There is some difference between the true negative stiffness and the negative stiffness. The force dropped immediately once the loading was applied on the true NS material, while the force would increase first and then decrease for the NS metamaterials when under loading. A more detailed introduction about the true NS

material can be found in recent research[77]. In this work, the magnets are respectively interlocked in the vertical supporting bar and the middle of the low supporting part of the cells. The interaction between the magnets in the vertical bar and the lower part is attractive and can decrease the force response of the filled cylindrical NS structure when applying the displacement-controlled loading. Thus, the filling magnet system is regarded as a type of true NS filler. The embedded magnets, as shown in Fig. 3(e), are made of Neodymium Iron Boron (NdFeB), and their dimensions are 0.00475×0.00475×0.00475 m. The material properties of the magnets and the sponges will be introduced in detail in Section 5.

4. Simulation and experiment

Numerical simulations were employed in this study to verify the theoretical models. The finite element (FE) solution should match the requirement of the problem[78], and thus the commercial FE software, ABAQUS 2017, was employed to perform the numerical simulations. The 3D digital model of the cylindrical NS structure was built in the CATIA (V5R20) software and then was imported into the ABAQUS. Considering the snap-through and snap-back are both transient behaviors, a dynamic solver is applicable here. The 'Dynamic, Implicit' was therefore employed in the 'Create step', and two steps were respectively created for the simulation of loading and unloading tests on the cylindrical NS structures.

The deformation modes of the spatial beam element are dominated by bending and compression. The element C3D8R (an 8-node linear brick, reduced integration, hourglass control element) can well avoid the shear locking when under bending

deformation, and the calculation is easy to converge when with the C3D8R element in large deformation. Consequently, the element C3D8R is chosen in our numerical simulations. The mesh size of the structure was determined through convergence analysis. The mechanical properties of the cylindrical NS structure are mainly determined by the spatial beam elements. Thus, the mesh size of the beam parts is refined. The final approximate mesh sizes of the beam parts and the supporting parts were respectively set as 0.5 mm and 1.5mm to ensure accuracy and calculation efficiency.

The rigid platen was used to deform the structure, as shown in Fig. 4(a). The circular platen diameter is larger than that of the cylinder structure to ensure the applied load is evenly distributed on the top of the structure. The top of the cylindrical structure is tied with the rigid platen in response to possible multi-stable and pseudo-bistable behavior because these behaviors would cause the unloading process to fail. The base of the cylindrical structure was tied with the other rigid platen, which was fixed. The displacement-controlled loading was exerted on the reference point of the upper rigid platen. This reference point was also monitored during the loading-unloading process to generate the response of the cylindrical NS structures.

During the loading process, the spatial beams may contact the annular supporting part and penetrate through it, which may postpone the densified stage. To prevent the structure from penetrating, we use the hard contact to describe the interaction property along the normal direction. When the spatial beams contact the annular supporting parts, their relative shear movement is not entirely free. The surface friction of the urethane

elastomer cannot be neglected, and it will prevent the relative movement of the contacted parts. To describe the tangential behavior of these contacted surfaces, the friction coefficient was set as 0.4.

The material properties of the base material, urethane elastomer, are necessary for the FE simulation. The Young's modulus of the base material was tested through standard tensile test according to the ASTMD-412. The specimens and the testing equipment, an electronic universal testing machine (INSTRON 5569), are shown in Fig. 3(f) and (g), respectively. The true stress-strain response curve of the base material under tensile load is also displayed in Fig. 3(g), and the Young's modulus is set as 15 MPa. The data of the base material's density and the Poisson ratio, provided by the producer (WeNext Technology Co., Ltd., China), are 1200 kg/m^3 and 0.4.

The linear elastic and true NS filler in the cylindrical NS structure can both be simplified as the spring in the software ABAQUS, as shown in Fig. 2(b). The spring can be realized in the ABAQUS using the *'Springs/Dashpots'* or the *'Connector'*. Two 'Reference points' should be created as the endpoints of the spring, As shown in Fig. 4(a). The springs are filled in the cell element. Thus, the endpoints of the spring should be coupled with the spatial inclined beam's ridgeline and the lower supporting part's upper surface, respectively. The cell element embedded with a spring, as shown in Fig. 4(a), indicates that the element is filled. The filler's properties can be determined by defining its stiffness.

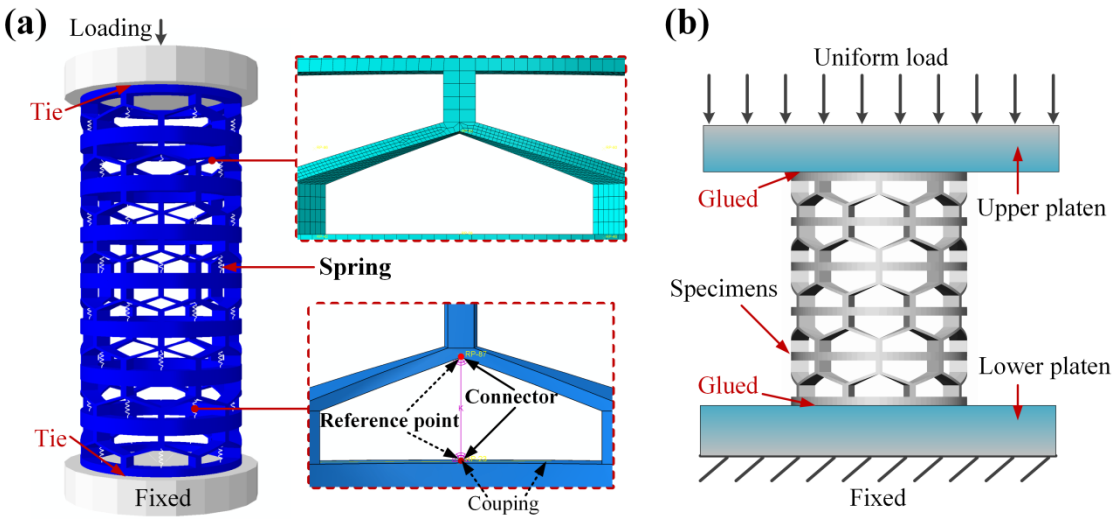

Fig. 4. (a) FE model of filled cylindrical NS structure; (b) experiment setups for loading-unloading tests.

Loading-unloading tests were performed to study the energy dissipation, energy absorption, and the basic mechanical properties of the filled and the unfilled cylindrical NS structures. The experiment setups are shown in Fig. 4(b), and the testing equipment is also the electronic universal testing machine (INSTRON 5569), as shown in Fig. 3(f). Considering the possible multi-stable or pseudo multi-stable behavior, the contact surfaces between the sample and the platens were glued. The crosshead speed was set as 3 mm/min. Moreover, the deformation processes of the samples under the loading-unloading test were videoed by the smart mobile phone (HORNOR 9X, produced by HUAWEI TECHNOLOGIES CO., LTD., China) to study the filler's influence on the deformation modes of the cylindrical NS structure.

5. Theory

5.1 Theory of single NS element

According to the previous research[47,51], building the theoretical model for the global NS mechanical metamaterials is dependent on the theoretical model of the local

NS element. In this section, a theoretical model for predicting the force-displacement response of the NS, spatial inclined beam element is built based on a recently presented method by Lei[79].

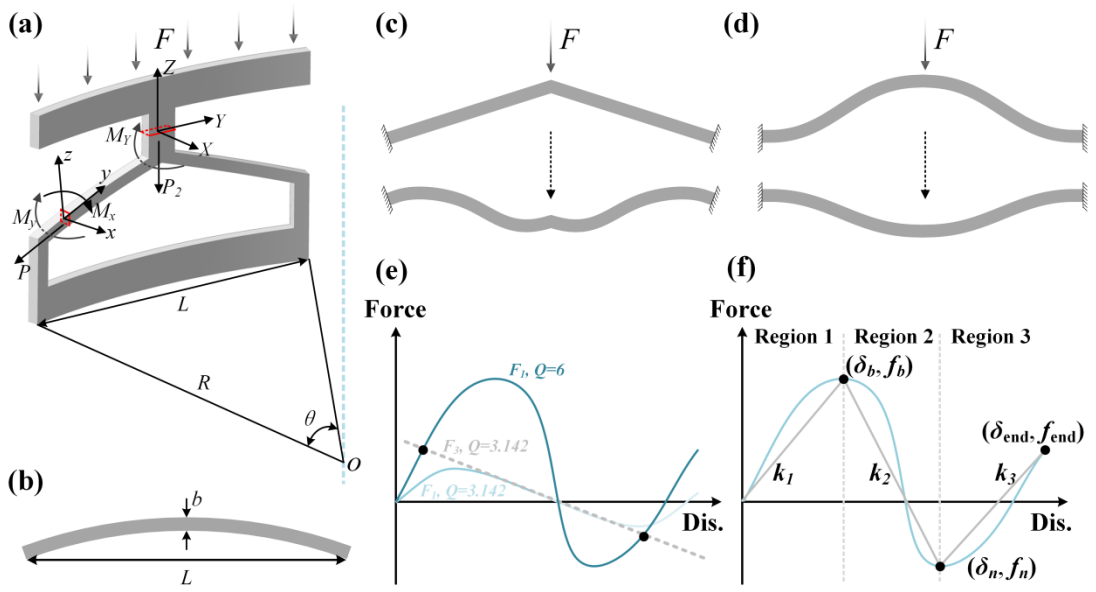

Fig. 5. (a) Force analysis of single NS beam element (spatial, inclined); (b) top view of single NS beam element. Snap-through process of (c) NS inclined beam element; (d) NS curved beam element. (e) Two solutions of spatial inclined beam element's force-displacement responses; (f) several key response points in NS response curve and trilinear model.

The investigated NS element, an inclined spatial beam, is presented in Fig. 5(a). The beam element's top view and snap-through process are shown in Fig. 5(b) and (c), respectively. The curved beam element, displayed in Fig. 5(d), can also be applied to construct the cylindrical NS structure in this paper. The shape of the inclined beam is relatively simpler than that of the curved beam and the manufacturing processes for the inclined beam are much easier[31]. Hence the inclined beam is selected in this study.

When the normalized applied force, F, is exerted on the central point of the planar inclined beam element, as shown in Fig. 5(c), it would deform and the relationship

between the normalized force, F, and the normalized displacement, Δ, can be expressed as[80]

$$F_1 = \frac{3}{2}\pi^4 Q^2 \Delta^3 - 36\pi^2 Q^2 \Delta^2 + 2\pi\Delta + 192Q^2\Delta \tag{1}$$

$$F_3 = 64\pi^2(1-\Delta) \tag{2}$$

where F_1 and F_3 are the two solutions of F.

$$Q = \frac{h}{t},\ \Delta = \frac{\delta}{h}, \tag{3}$$

where h and t are respectively the arch height and the thickness of the inclined beam element. δ is the displacement of the central point.

For the planar beam element with Q less than or equal to 3.124, its normalized force-displacement can be expressed by equation (1), and the diagram of the response curve is presented in Fig. 5(e), i.e., the light blue curve. The normalized force-displacement response can be divided into three parts for the planar beam element with Q greater than 3.124. The critical points of these three parts are highlighted with the black dots. The initial part and the third part can also be described by equation (1). The middle part should be described by equation (2). The diagram of the response curve of the planar beam element with Q greater than 3.124 is multi-segment, which is also presented in Fig. 5(e).

Based on the above theoretical model for the planar inclined beam element and the recently presented theoretical model[79] for the curved spatial beam, the theoretical model for predicting the force-displacement response of the spatial inclined beam element, as shown in Fig. 5(a), can be derived, and is

$$F_{1-\text{spatial}} = \frac{1}{K_1}\left(\frac{3}{2}\pi^4 Q^2 \Delta^3 - 36\pi^2 Q^2 \Delta^2 + 2\pi\Delta + 192Q^2\Delta\right), \tag{4}$$

$$F_{3-\text{spatial}} = \frac{1}{K_1}(64\pi^2(1-\Delta)), \tag{5}$$

where

$$K_1 = \left(\frac{\pi}{A\sin\frac{\pi}{A}}\right)^3. \tag{6}$$

More details about K_1 can be found in the literature[79].

The force-displacement response curves of the NS elements are usually described by the trilinear model. The schematic curve of the trilinear model is shown in Fig. 5(f), i.e., the gray line. The trilinear response curve consists of three key response points, the buckling point, the valley point, and the final point. For the spatial inclined beam element with Q less than or equal to 3.142, the normalized force and the normalized displacement responses of these three key response points can be calculated with Equation (4) and are as follow

$$\Delta_b = \frac{2}{3}\frac{12Q - \sqrt{-\pi^4 + 48Q^2}}{Q\pi^2}, \tag{7}$$

$$\Delta_n = \frac{2}{3}\frac{12Q + \sqrt{-\pi^4 + 48Q^2}}{Q\pi^2} \tag{8}$$

$$\Delta_{\text{final}} = \frac{160}{\pi^4}, \tag{9}$$

$$F_b = F_{1-\text{spatial}}\left(\frac{2}{3}\frac{12Q - \sqrt{-\pi^4 + 48Q^2}}{Q\pi^2}\right), \tag{10}$$

$$F_n = F_{1-\text{spatial}}\left(\frac{2}{3}\frac{12Q + \sqrt{-\pi^4 + 48Q^2}}{Q\pi^2}\right), \tag{11}$$

$$F_{\text{final}} = \frac{30720}{K_1\pi^4}. \tag{12}$$

When $Q > 3.142$, the normalized force and the normalized displacement responses of the three key response points can be calculated with Equation (4) and (5). The expressions of these key response points' normalized force and displacement are as follow

$$\Delta_b = \frac{2}{3} - \frac{2}{3}\sqrt{1-\frac{\pi^2}{Q^2}}, \tag{13}$$

$$\Delta_n = \frac{2}{3} + \frac{2}{3}\sqrt{1-\frac{\pi^2}{Q^2}}, \tag{14}$$

$$\Delta_{\text{final}} = \frac{5}{3}, \tag{15}$$

$$F_b = \frac{64\pi^2}{K_1}\left(\frac{1}{3} + \frac{2}{3}\sqrt{1-\frac{\pi^2}{Q^2}}\right), \tag{16}$$

$$F_n = \frac{64\pi^2}{K_1}\left(\frac{1}{3} - \frac{2}{3}\sqrt{1-\frac{\pi^2}{Q^2}}\right), \tag{17}$$

$$F_{\text{final}} = \frac{320}{K_1}. \tag{18}$$

The normalized force, F, and the normalized displacement, Δ, can be converted to the force, f, and displacement, δ, through

$$\delta = \Delta h,\ f = F\oint \frac{EIh}{L^3}, \tag{19}$$

where $I = \frac{t^3}{12}$, and $L = R + \delta R,\ \delta R \in (0, b)$.

Based on the three key response points (δ_b, f_b), (δ_n, f_n) and $(\delta_{\text{final}}, f_{\text{final}})$, the response curve of the NS element can be presented, and the model for the NS metamaterial can be built. In the next section, the theory for predicting the loading-unloading response of the NS metamaterial will be introduced in detail.

5.2 Theory of multi-layer structure

According to the previous research[47], the force-displacement response of an NS structure with *n* elements in series when under loading-unloading test can be described by the diagram, as shown in Fig. 6(b). The displacement and the force for each buckling point, marked by the black dots, in the loading path can be expressed as

$$\Delta_{bi} = n\delta_b + is_b,\ i = 0,\ 1,\ 2, \cdots,\ n-1, \tag{20}$$

$$f_{bi} = f_b,\ i = 0,\ 1,\ 2,\ \cdots,\ n-1, \tag{21}$$

where Δb_i and f_{bi} are the displacement and the force for the $(i+1)$-th buckling point. δ_b and f_b are the displacement and force at the buckling point of the NS element's force-displacement response, and can be obtained from the expressions in the above section. s_b represents the distance between the two adjacent buckling points and can be expressed as

$$s_b = \delta_m - \delta_b, \tag{22}$$

where δ_m is

$$\delta_m = \begin{cases} \dfrac{f_b - f_n}{k_3} + \delta_n, & f_{end} \geq f_b \\ \delta_{end}, & f_{end} < f_b \end{cases}. \tag{23}$$

k_3 is the equivalent stiffness of the NS element in region 3, as shown in Fig. 6(a).

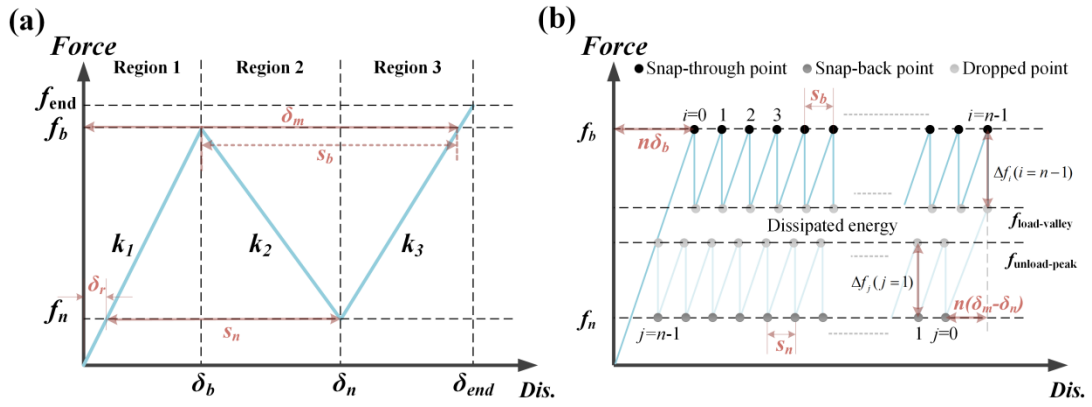

Fig. 6. (a) Trilinear response curve of single layer cylindrical NS structure; (b) diagram of cylindrical NS structure's loading-unloading response curves (multilinear response curve).

When the cylindrical NS structure is under compression via the electronic universal testing machine, the loading on the NS structure is displacement-controlled. In contrast, the loading on the buckling element from other elements is force-controlled from a local perspective. Thus, the local element is unstable in region 2, and the element would snap from region 1 to region 3 immediately when the local buckling occurs.

Therefore, the number of elements in a series can also be expressed as

$$n = n_1 + n_3, \tag{24}$$

where, n_1 and n_3 are the number of the elements in region 1 and region 3, respectively.

During the loading process, the elements in region 1 and 3 would backtrack once an element snapped from the buckling point into region 3. The real-time displacement for the elements in region 1 and 3 after the snap-through behavior are δ_1 and δ_3, respectively. Moreover, the parameters, δ_1 and δ_3, satisfy the following conditions.

$$\delta_r < \delta_1 < \delta_b \tag{25}$$

$$\delta_3 = \delta_n + \delta_3^{'} \tag{26}$$

where $\delta_3^{'}$ is the elements' local displacement component in region 3. δ_r is the displacement of a response point in region 1, whose force value equals f_n.

When one element (*i+1*) snapped through, the transient displacement of the element is $D_{i-\text{snapthrough}}$. The transient displacements of other elements in region 1 and 3 are D_{i-1} and D_{i-3}, respectively. It can be inferred that the increase in deformation of the *(i+1)*-th buckled element equals the sum of the deformation reduction of the other elements in region 1 and 3, thus,

$$(n-i-1)D_{i-1} + iD_{i-3} = D_{i-\text{snapthrough},} \tag{27}$$

where

$$D_{i-\text{snapthrough}} = \delta_n - \delta_b + \delta_3^{'}. \tag{28}$$

$\delta_3^{'}$ can also be expressed as

$$\delta_3^{'} = \delta_m - \delta_n - D_{i-3}. \tag{29}$$

According to the Eq. (27-29), we can deduce

$$(n-i-1)D_{i-1}+(i+1)D_{i-3}=s_b. \tag{30}$$

The elements are in series when under compression, thus, the transient changes of the force, Δf_i, for elements in region 1 and region 3 during the snap-though behavior are same with each other. Δf_i can be expressed as

$$\Delta f_i=\begin{cases} D_{i-1}k_1=D_{i-3}k_3,\ F_{end}\geqslant F_b \\ D_{i-1}k_1=D_{i-3}k_3+F_b-F_{end},\ F_{end}<F_b \end{cases}. \tag{31}$$

According to the Eq. (30-31), the transient displacement and drop force of the element in region 1 can be deduced, and are as follow

$$D_{i-1}=\begin{cases} \dfrac{s_b}{(n-i-1)+(i+1)\frac{k_1}{k_3}},\ F_{end}\geqslant F_b \\ \dfrac{s_b+(i+1)\frac{F_b-F_{end}}{k_3}}{(n-i-1)+(i+1)\frac{k_1}{k_3}},\ F_{end}<F_b \end{cases}. \tag{32}$$

$$\Delta f_i=D_{i-1}k_1. \tag{33}$$

Therefore, the force value of the valley point in loading path can be calculated by subtracting the transient drop force from the buckling force, and is as follow

$$f_{\text{load}-\text{valley}}=f_b-\Delta f_i. \tag{34}$$

The displacement of the *(i+1)*-th valley point equals the displacement of the *(i+1)*-th buckling point in the loading path because the snap-through behavior is a dynamic process. In summary, the coordinate of the *(i+1)*-th buckling point and the corresponding valley point in the loading path, as shown in Fig. 6(b), is $(\Delta_{bi},\ f_b)$ and $(\Delta_{bi}, f_{\text{load}-\text{valley}})$. Δ_{bi} and $f_{\text{load}-\text{valley}}$ can be calculated via the Eq. (20) and Eq. (34), respectively. f_b is the buckling force of the element and can be calculated via the expressions in Section 5.1.

The diagram of the NS metamaterial's unloading response is also displayed in Fig. 6(b). Contrary to the loading process, the elements in region 3 snap-back into region 1 gradually in the unloading path. The snap-back point and the following peak point are respectively marked through dark gray and light gray dots, as shown in Fig. 6(b).

The distance from the unloading-start point to the first snap-back point is $n(\delta_m - \delta_n)$. The distance from the unloading-start point to the (*j+1*)-th snap-back point can be expressed as

$$\Delta_{bj} = n(\delta_m - \delta_n - D_{n-1}) + js_n,\ j = 0,\ 1,\ 2, \cdots,\ n-1, \tag{35}$$

where

$$s_n = \begin{cases} \delta_n - \delta_r,\ f_n > 0 \\ \delta_n,\ f_n \leqslant 0 \end{cases}, \tag{36}$$

$$\delta_r = \frac{F_n}{k_1}. \tag{37}$$

Similar to the loading process, when one element (*j+1*) snapped back from region 3 to 1, the transient displacement of the element is $D_{j-\text{snapback}}$. The transient displacements of other elements in region 1 and 3 are D_{j-1} and D_{j-3}, respectively. It can be inferred that the change in deformation of the *(j+1)*-th buckled element equals the sum of the deformation change of other elements in region 1 and 3, thus

$$jD_{j-1} + (n-j-1)D_{j-3} = D_{j-\text{snapback}}, \tag{38}$$

where

$$D_{j-\text{snapback}} = \delta_n - \delta_b + D_{j-1}, \tag{39}$$

The elements are in series, thus, the forces of the elements in region 1 and region 3 are same with each other, thus

$$\Delta f_i = \begin{cases} D_{i-1}k_1 = D_{i-3}k_3,\ F_n \geqslant 0 \\ D_{i-1}k_1 = D_{i-3}k_3 + F_n,\ F_n < 0 \end{cases}. \tag{40}$$

According to the Eq. (38-39), we can deduce

$$D_{j-1} = \begin{cases} \dfrac{s_n}{(j+1)+(n-j-1)\frac{k_1}{k_3}},\ F_n \geqslant 0 \\ \dfrac{s_b + (n-j-1)\frac{F_n}{k_3}}{(j+1)+(n-j-1)\frac{k_1}{k_3}},\ F_n < 0 \end{cases}. \tag{41}$$

The force value of the peak point following the snap-back point can be calculated by

$$f_{\text{unload}-\text{peak}} = f_n + \Delta f_i, \tag{42}$$

where

$$\Delta f_j = D_{j-1}k_1. \tag{43}$$

In summary, the coordinate of the (j+1)-th snap-back point is $(n\delta_b + ns_b - \Delta_{bj},\ f_n)$, and the coordinate of the corresponding peak point is $(n\delta_b + ns_b - \Delta_{bj},\ f_{\text{unload}-\text{peak}})$. The parameters in the coordinate expressions can be calculated through the Eq. (35-43) and some expression in the above section.

Utilizing these key points in the response curve, i.e., the buckling point, the snap-back point, and their following valley and peak points, the force-displacement response curve of the NS mechanical metamaterials under loading and unloading conditions can be obtained. Additionally, the theory in this section is not only applicable for the presented cylindrical NS structure in this manuscript but is also helpful to characterize other kinds of NS mechanical metamaterials.

5.3 Theory of NS mechanical metamaterial with filler

In this section, the theory to investigate the NS mechanical metamaterials with different filling materials are presented. As shown in Fig. 1, the linearly elastic filler

can be simplified as a spring. The true negative stiffness filler is also linearly elastic through its stiffness is negative. The visco-hyperelastic filler is relatively complex and can be regarded as a nonlinear spring coupled with a dashpot. The fillers are all in parallel with the NS elements. Therefore, several essential response quantities of the filled NS element when under compression can be expressed as

$$\delta_{b-\text{filler}} = \delta_b, \tag{44}$$

$$\delta_{n-\text{filler}} = \delta_n, \tag{45}$$

$$\delta_{\text{final}-\text{filler}} = \delta_{\text{filler}}, \tag{46}$$

$$f_{b-\text{filler}} = \begin{cases} f_b + \delta_b k_{\text{filler}} \begin{cases} k_{\text{filler}} > 0, \text{ filler is lenearly elastic} \\ k_{\text{filler}} < 0, \text{ filler is true negative stiffness} \end{cases} \\ f_b + f_{\text{sponge}}(\delta_b), \text{ filler is viscohyperelastic (sponge)} \end{cases}, \tag{47}$$

$$f_{n-\text{filler}} = \begin{cases} f_n + \delta_n k_{\text{filler}} \begin{cases} k_{\text{filler}} > 0, \text{ filler is lenearly elastic} \\ k_{\text{filler}} < 0, \text{ filler is true negative stiffness} \end{cases} \\ f_n + f_{\text{sponge}}(\delta_n), \text{ filler is viscohyperelastic (sponge)} \end{cases}, \tag{48}$$

$$f_{\text{final}-\text{filler}} = \begin{cases} f_{\text{final}} + \delta_{\text{final}} k_{\text{filler}} \begin{cases} k_{\text{filler}} > 0, \text{ filler is lenearly elastic} \\ k_{\text{filler}} < 0, \text{ filler is true negative stiffness} \end{cases} \\ f_{\text{final}} + f_{\text{sponge}}(\delta_{\text{final}}), \text{ filler is viscohyperelastic (sponge)} \end{cases}, \tag{49}$$

where $f_{b-\text{filler}}$, δ_b, $f_{n-\text{filler}}$, δ_n, $f_{\text{final}-\text{filler}}$, δ_{fianl} represent the force and displacements of the three key response points in the filled NS element's force-displacement response curve, i.e., the buckling point, the valley point, and the end point. k_{spring} is the stiffness of the filler. f_{sponge} is the force contributed by the visco-hyperelastic filler, and its calculation depends on the constitutive relation of the sponge. The parameters, f_b, δ_b, f_n, δ_n, f_{final}, δ_{fianl} in Eq. (44-49) can be calculated through expressions in Section 5.1, and mechanical response of the filled NS structures can be obtained by

submitting parameters $f_{b-\text{filler}}$, δ_b, $f_{n-\text{filler}}$, δ_n, $f_{\text{final}-\text{filler}}$, δ_{fianl} to expressions in Section 5.2.

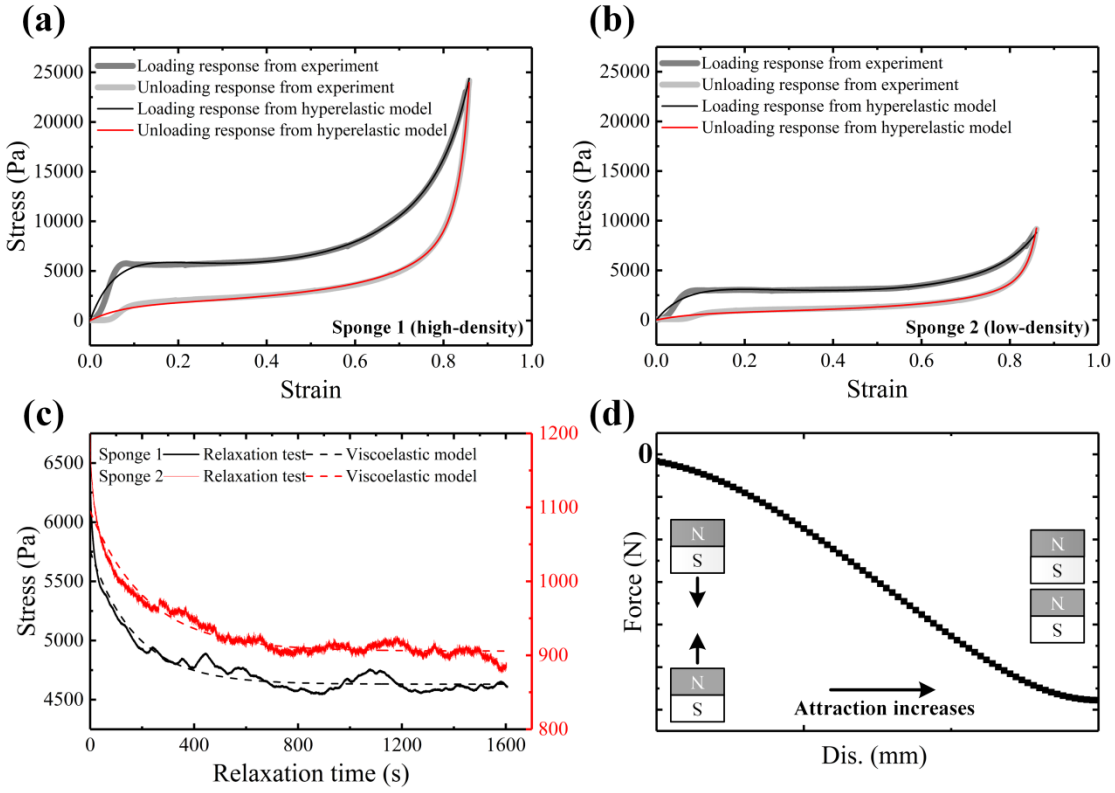

Fig. 7. Experimental loading-unloading response curves and corresponding fitting curves for (a) sponge 1 (high-density); (b) sponge 2 (low-density); (c) relaxation response curves and corresponding fitting curves of sponge 1 and 2. (d) Schematic force-displacement response curve of magnets system with particular configuration.

In this study, Ogden's model[81] was employed to describe the loading-unloading response of the polyurethane sponge. Ogden's model is as follows.

$$\sigma_{\text{sponge}}(\varepsilon) = 2(1-\varepsilon)^{-1}\sum_{1}^{3}\frac{\mu_k}{\alpha_k}\left[(1-\varepsilon)^{\alpha_k}-1\right], \tag{50}$$

where σ_{sponge} and ε represent the stress and strain, respectively. μ_k and α_k are the parameters, which can be obtained via fitting the sponge's response curve from experiments. The experiment response curve of polyurethane sponge (type 1 and type

2) under loading-unloading test and the corresponding fitting curves are shown in Fig. 7(a) and (b), respectively. The details of the loading-unloading test can be referred in the literatures[81,82].

As shown in Fig. 7(a) and (b), the experiment response curves and the fitting curves are in good agreement, indicating that Ogden's model is applicable in the description of the polyurethane sponge in large deformation. The fitting parameters of the loading-unloading response curves for sponge 1 and 2 are all listed in Table 2.

Tab. 2. Ogden's model parameter results for sponge 1 and sponge 2.

——	——	μ_1	α_1	μ_2	α_2	μ_3	α_3
Sponge 1	Loading	-11.71	-1.82	9300	4.16	-69830	18.63
	Unloading	-5700	15.35	-5739	15.35	-0.171	-5.27
Sponge 2	Loading	3893	2.99	369.70	109.90	-32230	16.80
	Unloading	-0.018	-5.85	118.40	89.29	-4706	14.29

Submitting the parameter values in Tab. 2 into Eq. (50), the expressions describing the stress-strain response of the polyurethane sponge (type 1 and type 2) can be obtained. With the sponge's stress-strain model, the f_{sponge} can be expressed as

$$f_{\text{sponge}} = \sigma_{\text{sponge}}(\varepsilon)\, s_{\text{area}}, \tag{51}$$

where s_{area} is the horizontal cross-section area of the filler. As shown in Fig. 2 (b), the horizontal cross-section area varies from the top to the bottom of the filler. Here, we assume that the effective cross-section area is a quarter of the horizontal cross-section area, which is the vertical projection of the inclined spatial beam. The basis of the assumption will be introduced in the next section. The effective cross-section area is

$$s_{\text{area}-\text{effective}} = \frac{\pi (R+b)^2 - \pi R^2}{4A} - \frac{3}{4} tb. \tag{52}$$

Based on Eq. (44-52), the critical parameters of the element filled with sponge can be calculated, and then the structure's mechanical response can be obtained by submitting these critical parameters into the expressions in Section 5.2.

The true NS behavior is a particular case of the NS behavior, which exhibits a negative tangent modulus once the loading is applied. The true NS system is usually at a neutral equilibrium state. The magnets system can exhibit the true NS behavior due to the internal attractive interaction. According to the previous researches[67], the attraction interaction of the magnets system under displacement-controlled loading can be demonstrated by Fig. 7(d). The response of the magnet system is similar to that of spring with linear, negative stiffness. Therefore, the magnets system was employed here to demonstrate the true NS filler's influence on the response of the cylindrical NS structure.

6. Results and discussion

In this section, the basic mechanical properties and the energy dissipation capacity of the filler-free and filled cylindrical NS structure are systematically investigated. The results from different methods are compared and analyzed. The influence of the different filling materials on the cylindrical NS structure's mechanical response is also analyzed in detail.

6.1 Mechanical properties of unfilled cylindrical NS structure

The theory for the NS element, as shown in Fig. 5(a), was verified with experiment[65] and the simulation results. The comparison of the mechanical response of

the single layer, cylindrical NS structure between experiments, simulations, and theory is shown in Fig. 8. It should be noticed that the response results in Fig. 8 are all for a single layer structure rather than the NS element since it is hard to test or simulate the mechanical response of the single element due to its complex boundary conditions. Thus, the single layer, cylindrical NS structures were employed here. The single layer structure is composed of A elements, and the mechanical response for the single layer structure is achievable based on the theory for the NS elements. Here, several samples (single layer) with different structural sizes are studied and compared, and their dimensions are listed in Tab. 3.

Tab. 3. Structural parameters of samples of single layer cylindrical NS structure.

	h (mm)	t (mm)	R (mm)	b (mm)	A	n
Sample 1	6	1.5	40	10	7	1
Sample 2	4	1.5	40	10	8	1
Sample 3	6	1.5	40	10	8	1
Sample 4	4	1.5	40	10	9	1

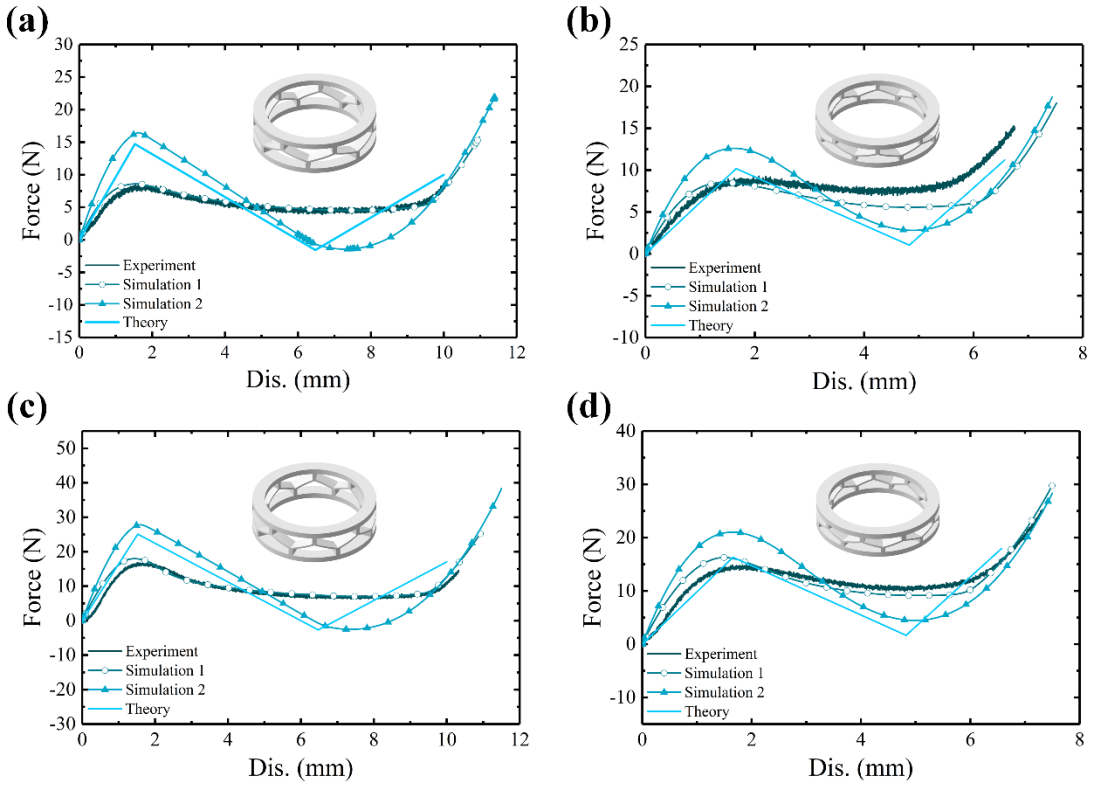

Fig. 8. Comparison of force-displacement response curves from experiments, theory, and simulations for single layer cylindrical NS structure when under uniaxial compression: (1) sample1; (2) sample 2; (3) sample 3; (4) sample 4.

The response results of Sample 1-4 from experiments, simulations, and the theory are presented in Fig. 8(a)-(d), separately. The response curves from different methods exhibit the same characteristics. However, significant errors do exist between the theory and the experiments. The experiment results are in good agreement with simulation 1 but differ from simulation 2. In contrast, the theoretical results are consistent with simulation 2 but show a remarkable difference with simulation 1 when with a great Q value. The difference is mainly caused by the simplified assumption in building the NS element's theoretical model, i.e., the out-of-plane deformation is neglected (the torques M_Y and M_y about the Y and y axis, as shown in Fig. 5(a), are neglected). However, the

out-of-plane deformation is evident for the cylindrical NS structure, especially for those with thin-wall and a big Q value. The out-of-plane deformation can weaken the structure's strength and stiffness. Therefore, the difference between experiments and theoretical methods exists. In simulation 2, the out-of-plane deformation of the cylindrical NS structure was constricted. Thus, the theoretical results and the simulation results are in good agreement, as shown in Fig. 8(a) and (c).

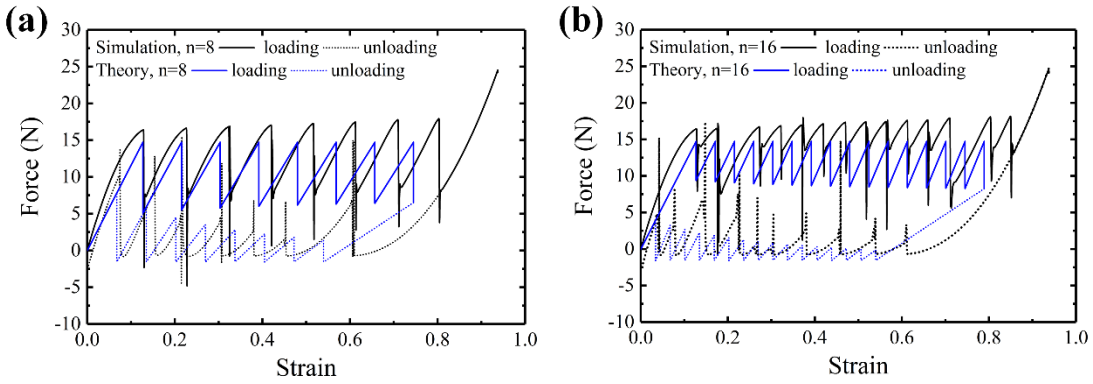

Fig. 9. Comparison of force-displacement response curves from theory and simulation: (a) n=8; (b) n=16. (A=7 mm, h=6 mm, t=1.5 mm, R=40 mm, b=10 mm).

Numerical simulations were employed to verify the theoretical model for the unfilled cylindrical NS structure. The loading-unloading response results for the unfilled cylindrical NS structures of different layer n (n=8 and n=16) from simulation and theory were compared in Fig. 9. Other parameter values of the cylindrical NS structures can be found in Tab. 1. The theoretical model can well describe the critical features of the response curves from simulations, whether in the curve form or the key points' coordinate values, and its accuracy is acceptable. The slight difference between the theory and the simulation is caused by the error in the theory for the NS element in Section 5.1. Overall, it can be concluded that the theory can well characterize the

loading-unloading response of the cylindrical NS structure.

As also observed from Fig. 9, the strength in the loading path and the minimum force in the unloading path remain constant as the layer, *n*, increases. In contrast, the force of the response points following the buckling point increases, and the force of the response points following the snap-back point decreases with the increment of *n*. The above changes further lead to the expansion of the enclosed area between the loading and unloading response curves, suggesting that the specific energy dissipation capacity improves as the layer, *n*, increases. This relationship between the cylindrical NS structure's layer number, *n*, and the specific energy dissipation capacity has been revealed in many previous researches[33,34,39,47,49] and can be applied in tuning the energy dissipation efficiency of the energy absorbing device.

Utilizing the above verified theoretical model, the influence of the structural parameters on the specific energy absorption (SEA) and specific energy dissipation (SED) capacity of the cylindrical NS structure is systematically studied and discussed. The effect of the *h/t* and *A* on the specific energy dissipation of the cylindrical NS structure with *n* equaling 16, 64, and 2000 is shown in Fig. 10(a). The absorbed energy was calculated by integrating the loading response curves from the minimum displacement to the densified displacement. The dissipated energy was calculated by integrating the enclosed area between the loading and the unloading response curves. The specific energy absorption, i.e., the energy absorption per unit volume, can be obtained by dividing the absorbed energy by the initial volume of the cylindrical NS structure. The calculation of the specific energy dissipation can follow the same way.

The initial volume of the cylindrical NS structure can be expressed as

$$V_{\text{initial}} = \pi\left(R+b\right)^2 H. \tag{1}$$

H is the height of the cylindrical structure.

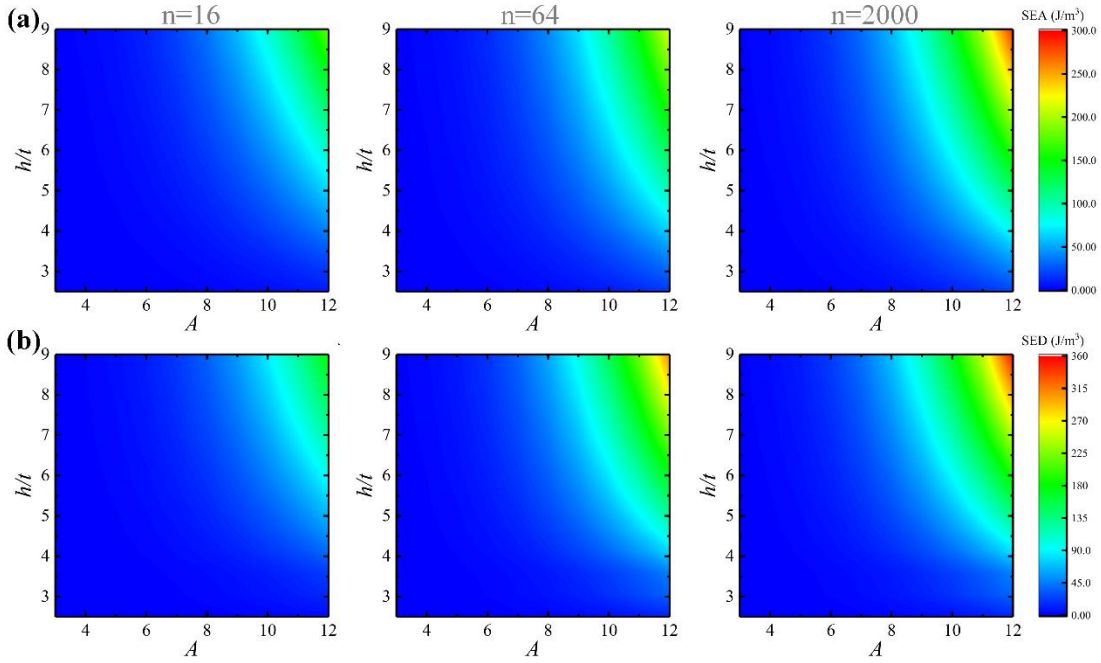

Fig. 10. Relationships between structural parameters (h/t and A) and (a) specific energy absorption (SEA) (n=16, n=64, n=2000); (b) specific energy dissipation (SED) (n=16, n=64, n=2000) of unfilled cylindrical NS structure. (R=40 mm, b=10 mm).

As shown in Fig. 10(a), when other parameters remain unchanged (these parameter values can be found in Tab. 1), the specific energy absorption and dissipation both increase as A or h/t (Q) increases. The specific energy absorption and dissipation increase steadily as the layer number increases, owing to that the serration in the loading-unloading response curves become shallower and denser as n increases, and the response curves become full, as reflected in Fig. 9.

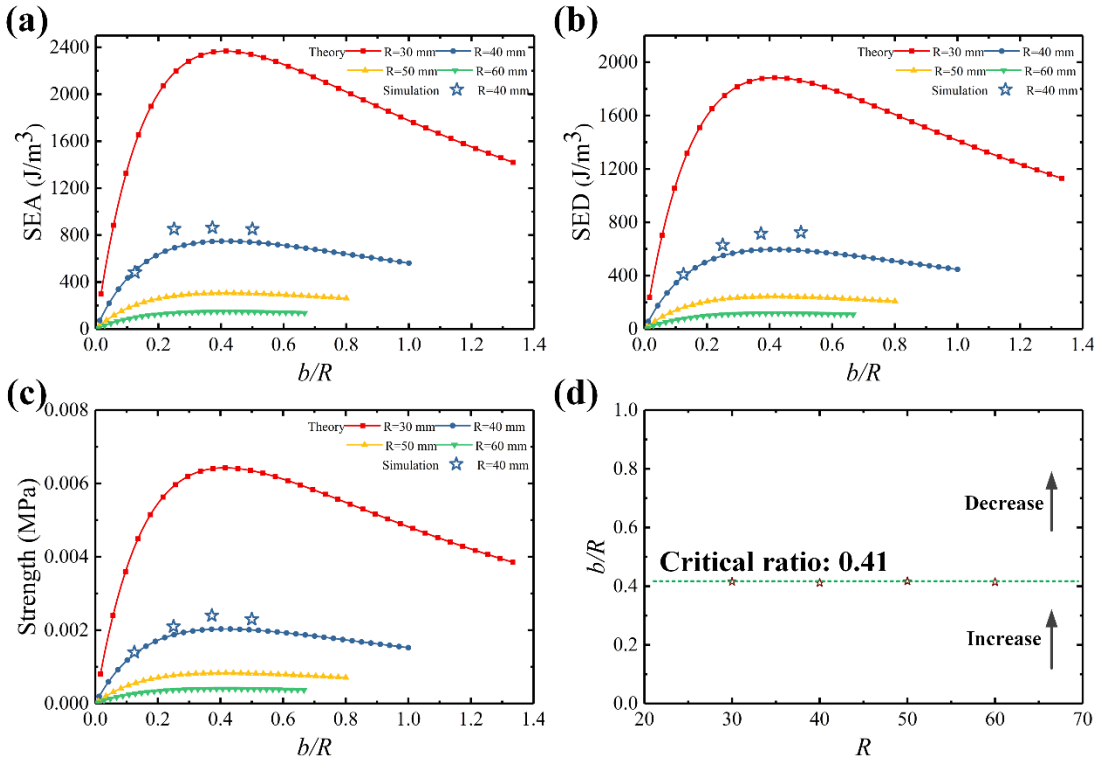

Fig. 11. Influence of parameter ratio (*b/R*) on the: (a) specific energy dissipation; (b) specific energy absorption; (c) strength, of cylindrical NS structure of *n*=8; (d) critical ratio of *b/R*.

According to the previous research[65], the thickness-diameter ratio greatly influences the mechanical properties of the cylindrical shell structures, but relevant research about cylindrical NS structures is lacking. Here, the influence of the thickness-diameter ratio, *b/R*, on the cylindrical NS structure's strength, specific energy absorption, and dissipation are studied, and the results are presented in Fig. 11. The specific energy absorption of the cylindrical NS structure increases first and then decreases as the ratio *b/R* increases whatever the internal radius *R* is. The specific energy dissipation and the strength also exhibit the same changing trend. Also, as we can see, the simulation results match well with the theoretical results.

According to the comparison, the critical ratio *b/R* between the different changing trends for the strength, specific energy dissipation, and absorption are completely

identical when the *R* is determined. The critical ratios *b/R* for the cylinder with different *R* are very close from the observation from Fig. 11(a)-(c). In order to study the relationship between the critical ratio and *R*, some data are extracted from Fig. 11(a)-(c) and illustrated in Fig. 11(d). The critical ratio *b/R* almost stays constant as the *R* increases and is about 0.41. The above relationships demonstrate that increasing the thickness-diameter ratio, *b/R*, can improve the mechanical properties, but there is a limit and it seems that 0.41 is the best setting for the ratio *b/R*.

6.2 Mechanical properties of cylindrical NS structure with linear elastic filler

In this section, the mechanical properties of the cylindrical NS structure with linear elastic filler are investigated through simulation and theory. The comparison of the response curves from simulation and theory between the filled and the unfilled cylindrical NS structure is shown in Fig. 12(a) and (b), respectively. The main parameter values of the filled structure can be found in Tab.1, and the stiffness of the linear elastic filler, i.e., the spring, is set as $-\frac{k_2}{2}$. The comparison results show that introducing the linear-elastic filler can significantly change the properties of the cylindrical NS structure. The stiffness of the filled structure improves compared to the unfilled one. The peak and the minimum force in the response curves are both enhanced after introducing the filler. Additionally, the increase of the minimum force is larger than that of the peak force. The length of the serrated stress plateau becomes short, i.e., the response entered the compacted stage earlier. These changes directly lead to the reduction of the enclosed area between the loading and the unloading response curves, indicating that the linear elastic filler would weaken the energy dissipation capacity of

the cylindrical NS structures.

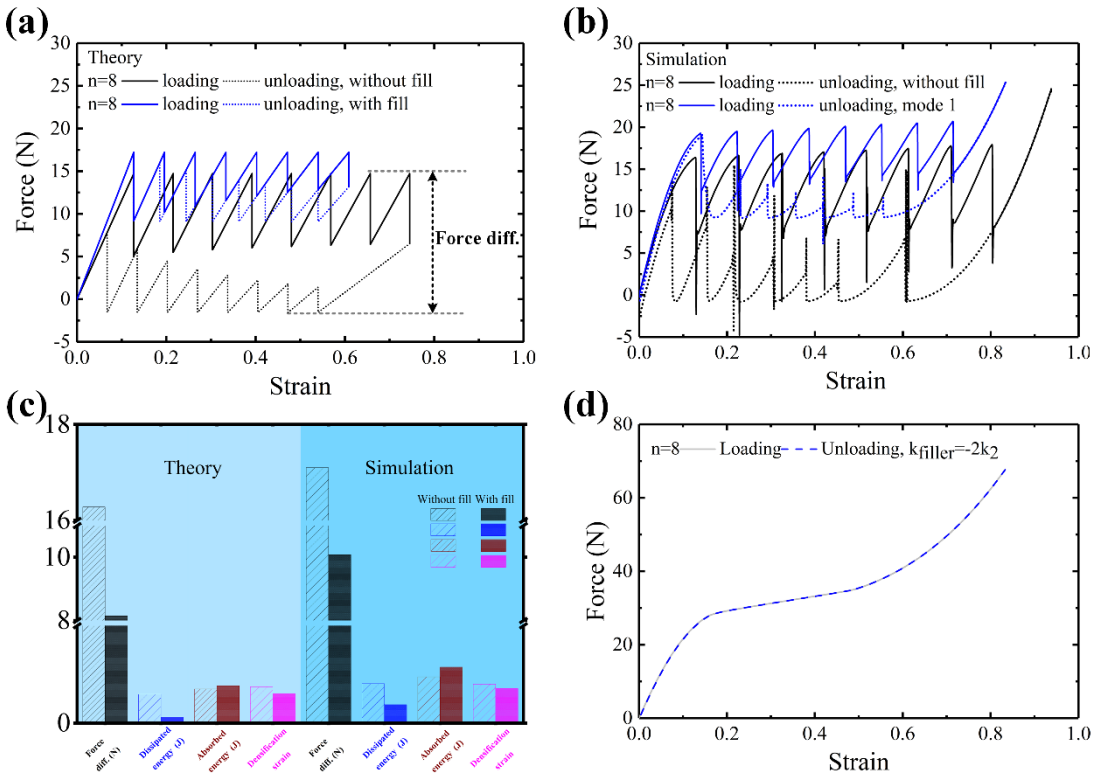

Fig. 12. Comparison of force-displacement response curves for filled and unfilled cylindrical NS structure (k_{filler}=-k_2/2) from: (a) theory; (b) simulation. (c) Comparison of each property for unfilled and filled cylindrical NS structure (k_{filler}=-k_2/2); (d) force-displacement response curves from simulation for filled cylindrical NS structure (k_{filler}=-2k_2). (A=7 mm, h=6 mm, t=1.5 mm, R=40 mm, b=10 mm, n=8).

In order to intuitively exhibit the influence of the filler, the force difference (peak force minus the valley force), the dissipated energy, the absorbed energy, and the densification strain of the filled and unfilled structure are all calculated out and compared in Fig. 12(c). The force difference and the densification strain decreased significantly and directly weakened the energy dissipation capacity. The absorbed energy increased, owing to the enhancement of the peak force. However, the significant decrease of the densification strain has a negative effect on the energy absorption

capacity, and therefore, once the promoting effect of the filler cannot offset the side effect, the energy absorption may also decrease. The further analysis of the filler's influence on the energy absorption capacity will be conducted in the following part. As also can be observed, the changing amplitude and trend of each property obtained from theory are very close to those from simulation. The response curves from the theoretical method are also almost consistent with the curves from the simulation, which indicates that the model can well describe the mechanical characteristic of this filled cylindrical NS structure and is of great accuracy.

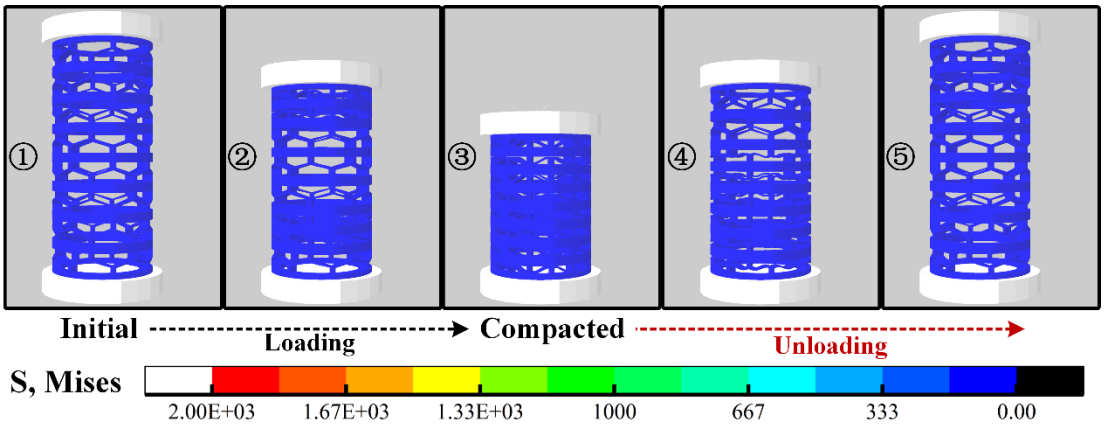

Fig. 13. Deformation processes from simulation for unfilled cylindrical NS structure.

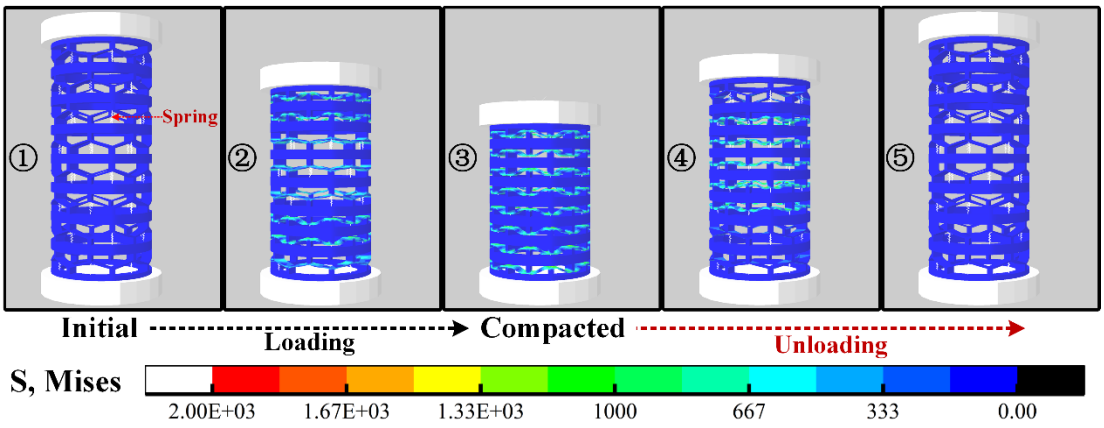

Fig. 14. Deformation processes from simulation for filled cylindrical NS structure (k_{filler}=-k_2/2).

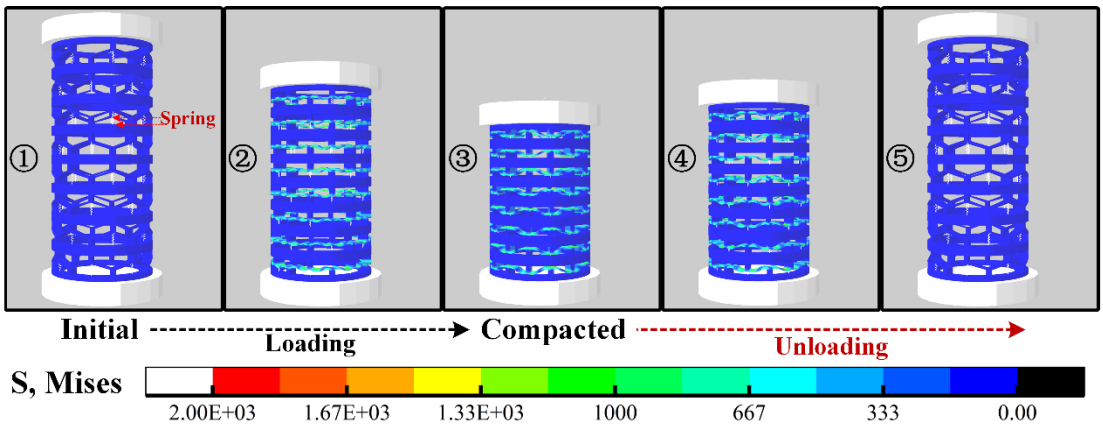

Fig. 15. Deformation processes from simulation for filled cylindrical NS structure (k_{filler}=-2k_2).

The deformation processes of the filled cylindrical NS structure with the linear elastic filler under loading-unloading from simulation are displayed in Fig. 14. The springs (marked in Fig. 14-①) deform with the deformation of the elements. The deformation mechanism of the filled cylindrical NS structure under the loading-unloading test remains constant as the unfilled one, as shown in Fig. 13, i.e., collapse (snap-through) layer by layer when under compression, and snap-back layer by layer in the unloading path. In order to retain the periodic snap-through and snap-back behavior after introducing the linear elastic filler, the stiffness of the filler (spring) should satisfy

$$k_{\text{spring}} < |k_2|. \tag{53}$$

This condition can prevent the element and the cylindrical structure from transforming to positive stiffness when introducing the filler. If the stiffness of the filler (spring) is not satisfied with the condition, Eq. (44), the cylindrical NS structure would become a system composed of nonlinear positive stiffness elements in series. The mechanical response and the deformation processes of the cylindrical structure are shown in Fig. 12(d) and Fig. 15, where the stiffness of the filler is set as $-2k_2$. It can be seen that the loading and unloading paths are almost overlapped, and the enclosed area between

the response curves, caused by the snap-back behavior, disappears. In addition, the elements in the series deform simultaneously, as shown in Fig. 15, like the series-connected springs. Consequently, the rational setting of the filler's stiffness is essential, and the excessive stiffness would fundamentally change the mechanical properties of the cylindrical NS structure.

The NS system with snap-through and snap-back behavior need to meet the following condition[39]

$$\left(\frac{n_1}{k_1}+\frac{n_3}{k_3}\right)^{-1} \leqslant k_2. \tag{54}$$

Introducing the filler brings big changes to $k_1,\ k_2,\ k_3$. Some structures may go against the Eq. (45) once with the filler and lose the energy dissipation function. Therefore, the stiffness of the filler also should satisfy

$$\left(\frac{n_1}{k_1+k_{\text{spring}}}+\frac{n_3}{k_2+k_{\text{spring}}}\right)^{-1} \leqslant k_2+k_{\text{spring}}. \tag{55}$$

Harnessing the theoretical model, the influence of the filler's stiffness on the cylindrical NS structure's energy absorption and dissipation capacity is further studied. The changing curves of the energy absorption and dissipation as the filler's stiffness increases are respectively presented in Fig. 16 (a) and (b). The normalized stiffness of filler is $\left|\frac{k_{\text{spring}}}{k_2}\right|$. The energy absorption would increase first and then decrease slightly for the NS structures with big Q (h=6). However, the energy absorption exhibits a monotonic increase for the NS structure with a small Q (h=4). As discussed above, the energy absorption capacity is mainly dominated by the plateau stress and the densification strain. Introducing filler has a positive effect on one factor but has a side effect on the other. Thus, two different changing trends in Fig. 16(a) are possible. The

energy dissipation capacity for NS structures with different parameters all attenuate with the increase of filler stiffness and would completely lose when the filler's stiffness increases to a specific limit. The disappearance of the energy dissipation function can be explained by Eq. (46), i.e., the filler prevented the snap-through and snap-back behavior. The simulation results in Fig. 16(a) and (b) are also verified by the simulation results. Obviously, the simulation results also capture the same changing trend.

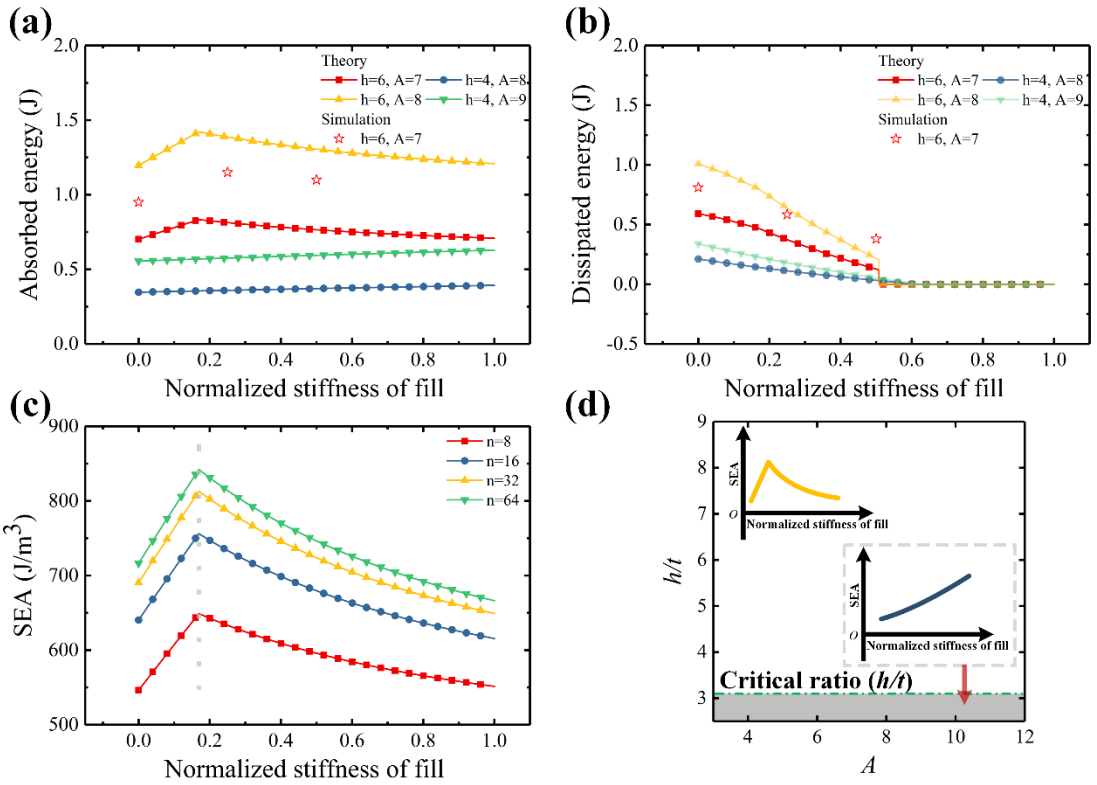

Fig. 16. Relationship between filler's stiffness and: (a) energy absorption capacity; (b) energy dissipation capacity. (c) Relationship between filler's stiffness and specific energy absorption (SEA) for structure with different *n,* (A=7, h=6 mm); (d) critical boundary of different changing trend for structure's energy absorption capacity. (t=1.5 mm, R=40 mm, b=10 mm).

The relationship between the filler's stiffness and the energy absorption capacity for NS structure with different n are also investigated. As shown in Fig. 16(c), the specific energy absorption also increases first and then decreases with the filler's

stiffness. Moreover, the critical value of the filler's stiffness for these different structures seems the same. Combined with the results presented in Fig. 16(a), it can be inferred that the changing trend of the energy absorption capacity is just related to the ratio Q (h/t).

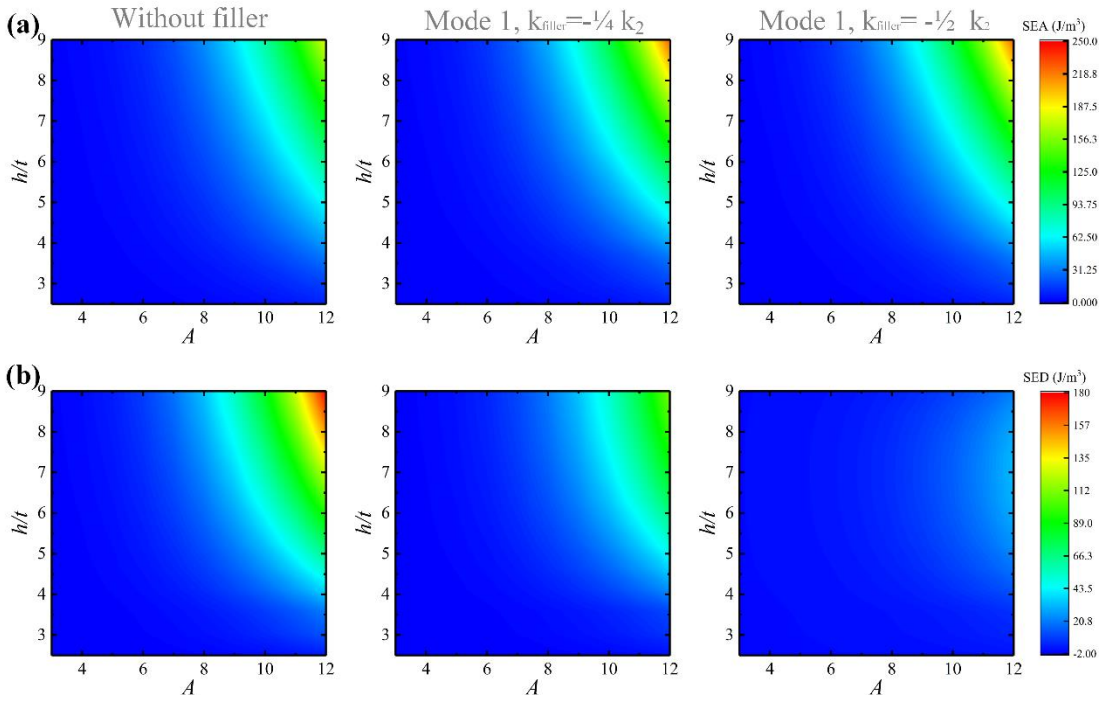

Fig. 17. Property comparison between unfilled cylindrical NS structure and filled cylindrical NS structure (k_{filler}=-$k_2/4$ and k_{filler}=-$k_2/2$): (a) comparison of specific energy absorption (SEA); (b) comparison of specific energy dissipation (SED). (n=16, R=40 mm, b=10 mm).

Based on the theory, the changing trend of the energy absorption capacity for filled NS structure of different parameters is studied, and the relevant results are illustrated in Fig. 16(d). The filled NS structure with geometric parameters located in the white region would exhibit the nonmonotonic trend on their energy absorption capacity, as described by the yellow curve in Fig. 16(d), while the filled NS structure with geometric parameters located in the grey region would exhibit the monotonic trend, as described by the deep blue curve. The critical ratio Q between these two different changing trends

is around 3.1.

The influence of the structural parameters on the mechanical properties of the filled cylindrical NS structure is also investigated through the theoretical method and then compared with the unfilled cylindrical NS structure. The influence of the parameters, *h/t* and *A*, on specific energy absorption and dissipation of the unfilled and the filled cylindrical NS structure with filler's equivalent stiffness equaling $-\frac{k_2}{4}$ and $-\frac{k_2}{2}$ is shown in Fig. 17. The relationships between the specific energy absorption and these parameters and between the energy dissipation and these parameters remain unchanged when introducing the linear elastic filler. The specific energy absorption and dissipation both increase with the increase of *h/t* and *A* for the unfilled and filled cylindrical NS structure. In addition to the phenomena above, the influence of the linear elastic filler, observed in Fig. 12 and 16, is also reflected in Fig. 17. The dissipation energy would decrease when introducing the filler and continuously decreases as the stiffness of the filler increases.

6.3 Mechanical properties of cylindrical NS structure with visco-hyperelastic filler

The layer number, *n*, has a significant influence on the NS structures' energy dissipation capacity and the energy dissipation mechanism. When the layer number, *n*, is small, such as *n*=1 and 2, there is no snap-back behavior during the load-unloading test. At this time, the energy dissipation is dependent on the structure's viscosity. While, the snap-back behavior would occur as the layer number, *n*, increases, and the energy dissipation mechanism transforms to 'twinkling'[49]. Here, the influence of the visco-

hyperelastic filler on the mechanical properties of the cylindrical NS structure with and without snap-back behavior are investigated.

The experimental response curves of the unfilled and filled cylindrical NS structure (n=1 and n=2) under the loading-unloading test are compared in Fig. 18(a) and (b). From the observation, snap-back behavior does not happen during the test of the unfilled cylindrical NS structures (n=1 and n=2), and the enclosed area between the loading and unloading response curves is tiny. The enclosed area between the loading and unloading response curves for the filled cylindrical NS structure is more extensive than that of the unfilled structure, which indicates that the energy dissipation capacity improves by filling the visco-hyperelastic sponge. Moreover, the initial stiffness and the strength of the filled cylindrical NS structure both increase with the filler's effect. The initial states and the deformed states of the unfilled and filled cylindrical NS structures (n=1 and n=2) are shown in Fig. 19(a) and (b).

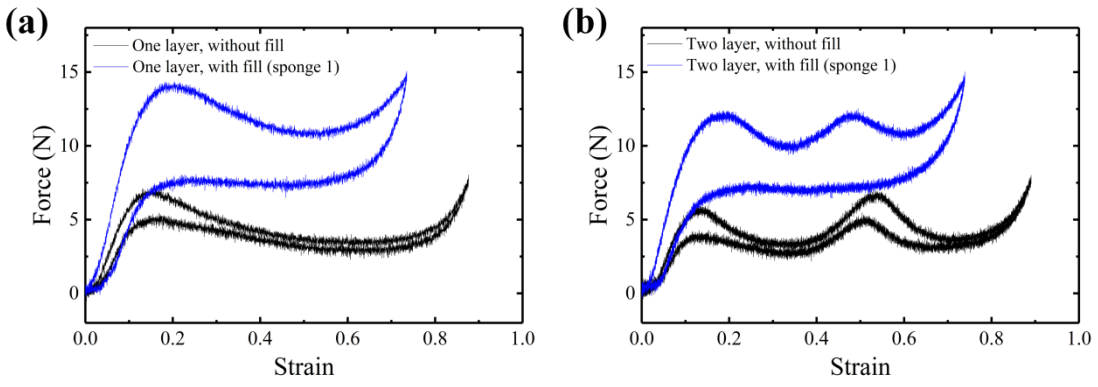

Fig. 18. Comparison of experimental loading-unloading response curves for unfilled cylindrical NS structure and filled cylindrical NS structure with visco-hyperelastic sponge: (a) n=1; (b) n=2.

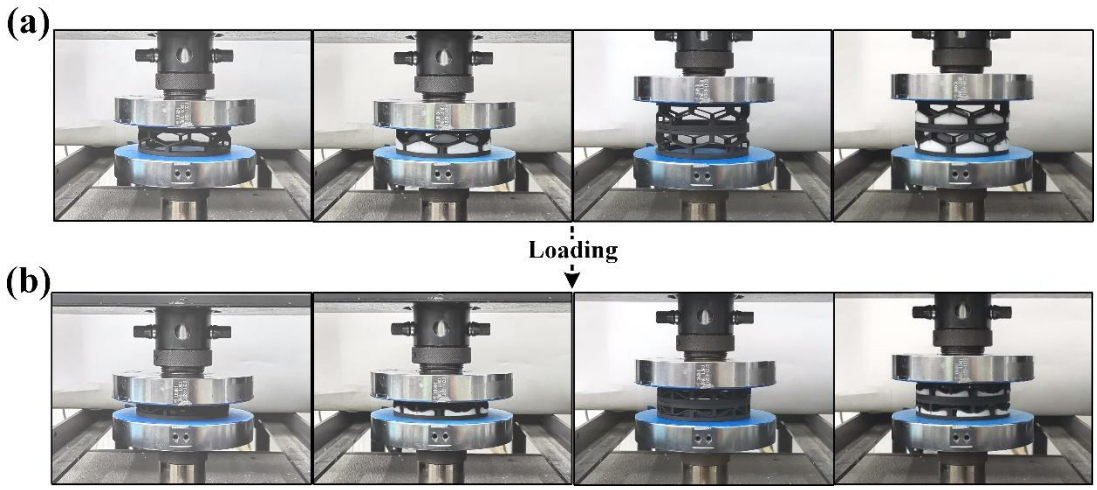

Fig. 19. (a) Initial states; (b) deformed states, of unfilled cylindrical NS structure (n=1), filled cylindrical NS structure (n=1), unfilled cylindrical NS structure (n=2), and filled cylindrical NS structure (n=2). (A=7 mm, h=6 mm, t=1.5 mm, R=40 mm, b=10 mm).

The dissipated energy by the filled cylindrical NS structure (n=1 and n=2) consists of two main components: the energy dissipated by the cylindrical NS structure and the energy dissipated by the filler. Therefore, the energy dissipation of the cylindrical NS structure without snap-back behavior would undoubtedly be improved by filling the visco-hyperelastic filler regardless of the filler's viscosity.

The influence of the visco-hyperelastic filler on the mechanical properties of the cylindrical NS structure with snap-back behavior is also investigated. The theoretical response results of the cylindrical NS structure without filler and with different visco-hyperelastic filler (sponge 1 and sponge 2) are compared in Fig. 20(a), and their experiment results are compared in Fig. 20(b). The cylindrical NS structure with snap-back behavior exhibits higher energy dissipation efficiency than that without snap-back behavior. The theoretical and the experimental results both show that the enclosed area between the response curves increases when filling the sponge. The initial stiffness, the

peak force, and the minimum force are all improved using the filler, while the stress plateau's length decreases. Although the theory can well describe the change brought by the filler, it does have inevitable errors compared to the experiment. The difference between the theory and the experiments is partly caused by the assumption about the effective cross-section area, s_{area}, in the derivation of the theoretical model in Section 5.3. On the other hand, the gel-casting fabrication method is not so stable and further increases the error.

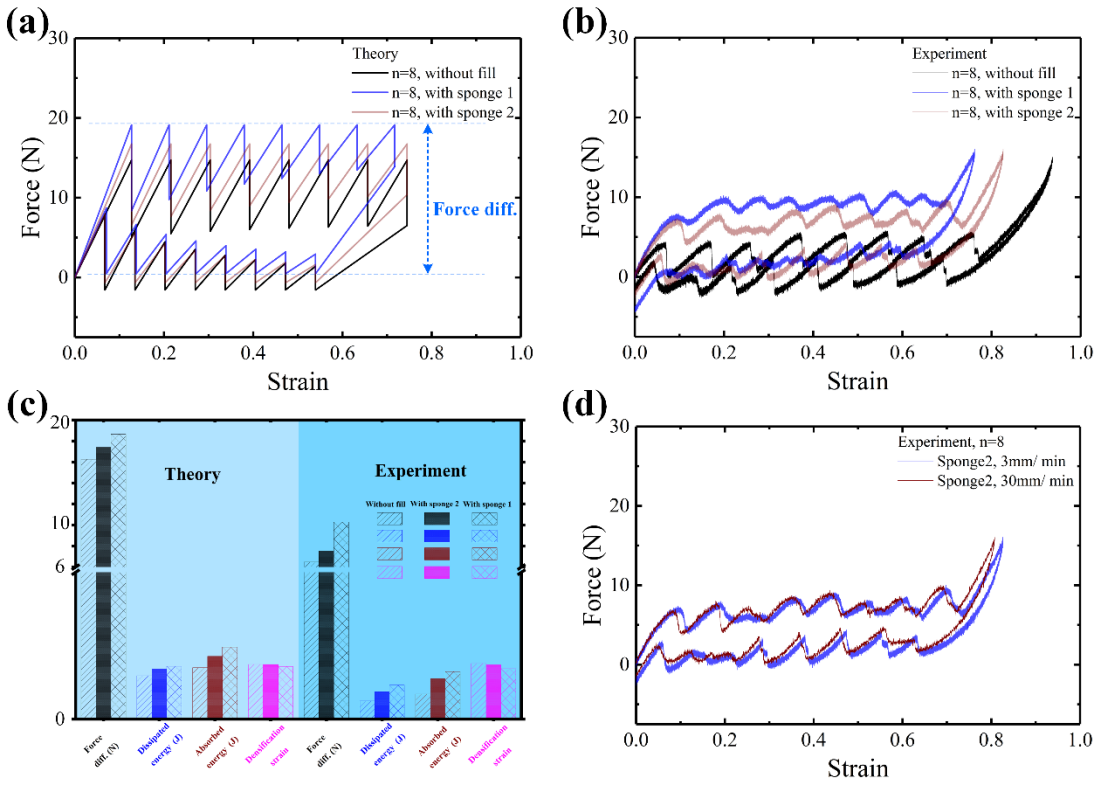

Fig. 20. Comparison of loading-unloading response curves from: (a) theory; (b) experiments, for filled cylindrical NS structure with different sponge and unfilled one. (c) Comparison of each property for unfilled and filled cylindrical NS structure; (d) loading-unloading response curves for filled cylindrical NS structure at different strain rate.

The force difference, energy absorption, energy dissipation, and the densification strain of the unfilled and filled cylindrical NS structure are compared in Fig. 20(c).

Revealed variation trend of each property by the theory is consistent with that from the experiments. The force difference, energy absorption, and energy dissipation all increase under the filler effect. In addition, as the filling sponge shifts from sponge 2 to sponge 1, these properties of the filled cylindrical structure continue to increase. According to the relaxation test results, shown in Fig. 7(c), the viscosity of the polyurethane sponge 2 is 2.96 MPa/s and is far smaller than that of sponge 1, which is 11.06 MPa/s (the viscosity can be achieved by fitting the relaxation response curves). The details of the relaxation tests and the model to fit the relaxation response curves can be found in the literatures[83]. The stiffness and the strength of sponge 1 are also greater than those of sponge 2, as shown in Fig. 7(a) and (b). Overall, the influence of the visco-hyperelastic filler on the NS structure would increase with the improvement of the sponge's mechanical performance.

Based on the comparison results of the filled structure with sponge 1 and 2, it can be concluded that the influence of the visco-hyperelastic filler on the cylindrical NS structure is seriously related to the characteristics of the filler, especially the filler's viscosity. It can also be inferred that the enhancement effect to the energy dissipation capacity would decrease and turn to negative gradually as the viscosity decreases. Moreover, the NS behavior would disappear if the stiffness of the filler is relatively large. Therefore, rational selection of the visco-hyperelastic filler is necessary for the optimization of the cylindrical NS structures. Notably, this is the difference in the visco-hyperelastic filler's influence on the cylindrical NS structure with and without snap-back behavior. The energy dissipation capacity of the structure without snap-back

behavior can undoubtedly be improved by filling the visco-hyperelastic filler regardless of the filler's properties. This difference is mainly caused by their different optimization mechanism. For the cylindrical NS structures with snap-back behavior, the visco-hyperelastic filler is applied to tune the snap-through and snap-back behavior and enhance the energy dissipation capacity, rather than only harnessing the visco-hyperelastic filler to dissipate energy directly as the filled cylindrical NS structure without snap-back behavior did.

The influence of the strain rates on the filled cylindrical NS structure with visco-hyperelastic filler is preliminarily studied through experiments. The experimental response curves of the filled cylindrical NS structure with sponge 2 under different loading speed, 3 mm/min and 30 mm/min, are compared in Fig. 20(d). The filled cylindrical NS structure with sponge 2 are not sensitive to the loading speeds, and the response curves from 3 mm/min and 30 mm/min are almost coincide with each other. There is no doubt that the influence of the strain rates is very complicated and the results reflected in Fig. 20(d) are not comprehensive. Considering that the focus of this study is on the quasi-static performance of the filled cylindrical NS structure, further study of the strain rate's effect will be conducted in our future research.

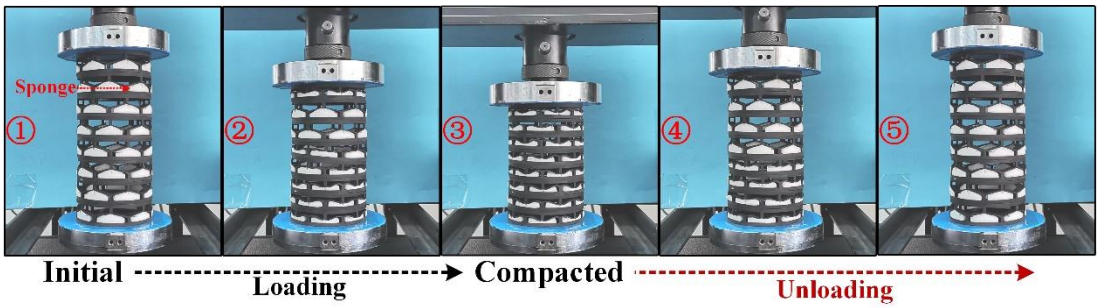

Fig. 21. Deformation processes from experiments for unfilled cylindrical NS structure when

under loading-unloading test. n=8.

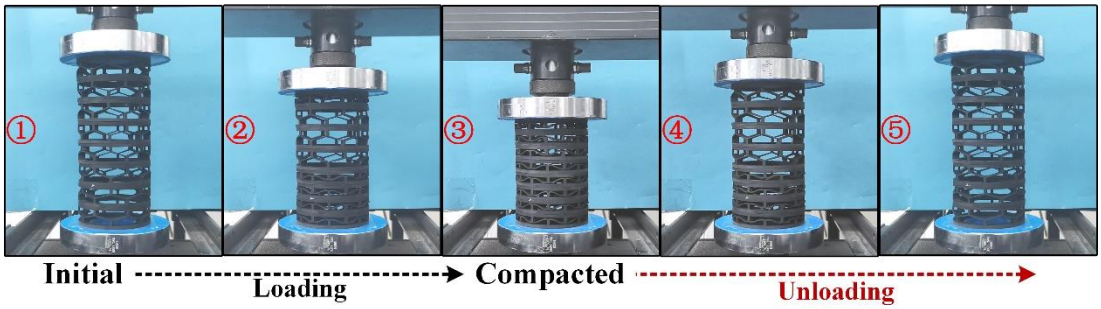

Fig. 22. Deformation processes from experiments for filled cylindrical NS structure with visco-hyperelastic sponge when under loading-unloading test. (n=8).

The deformation processes of the unfilled and the filled cylindrical NS structure with the polyurethane sponge under loading and unloading tests are displayed in Fig. 21 and 22. The filled polyurethane sponge brings no change to the deformation modes of the local cell element and the global cylindrical structure from the observation of the deformation processes. However, similar to the transformation of the deformation modes from Fig. 14 to 15, the global deformation mode, i.e., periodic snap-through and snap-back, would also change once the filler is of great stiffness.

The influence of the visco-hyperelastic filler on the specific energy absorption and the specific energy dissipation for the filled cylindrical NS structure with different n is investigated, and the results are presented in Fig. (23). The specific energy absorption and dissipation of the filled and the unfilled cylindrical NS structure increases with the increment of layer number n, and the growth rate gradually slows down. This variation trend is in accordance with the characteristics of the NS structures. The filled cylindrical NS structure with sponge 1 possessed better specific energy absorption and dissipation performance regardless of layer number n. Moreover, layer number n enlarges the

difference of these performances between the filled structure with different sponges and between the filled and unfilled structures, which indicates that the visco-hyperelastic filler has a more significant promotion on the specific energy absorption and dissipation for the cylindrical NS structure with more layers. The promotion effect would also be enhanced with the improvement of the filler's mechanical performance.

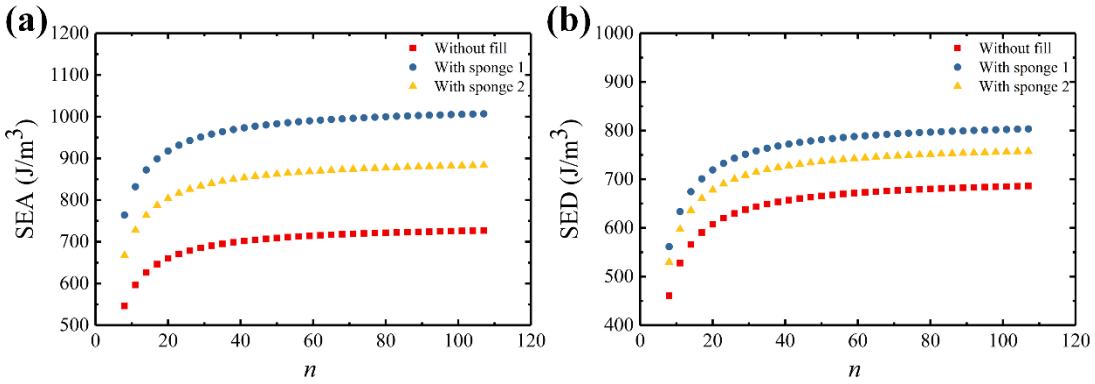

Fig. 23. Influence of layer number n on: (a) specific energy absorption; (b) specific energy dissipation, for unfilled and filled cylindrical NS structure. (A=7 mm, h=6 mm, t=1.5 mm, R=40 mm, b=10 mm).

Mechanical properties of the filled cylindrical NS structure of different structural parameters are also studied through theory, and the results are displayed in Fig. 24. The white region indicates that the negative stiffness property of the structure is lost when filled with the sponge because the filler's stiffness is too big. In the rest color region, the cylindrical NS structure's specific energy absorption and dissipation increase a lot when with the filler. In addition, the influence of the structural parameters on the mechanical properties of the filled cylindrical NS structure almost remains constant as the unfilled ones. Overall, the stiffness match between the filler and the cylindrical NS structure is the key to improve the performance.

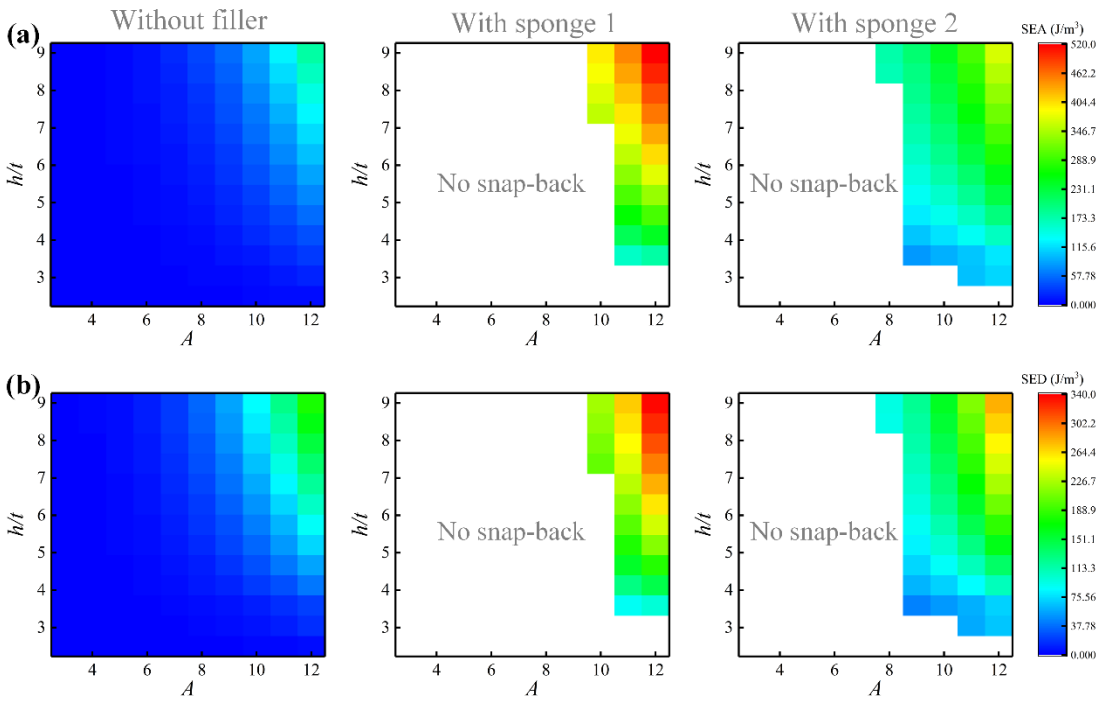

Fig. 24. Property comparison between unfilled cylindrical NS structure and filled cylindrical NS structure (sponge 1 and sponge 2): (a) comparison of specific energy absorption (SEA); (b) comparison of specific energy dissipation (SED). (n=16, R=40 mm, b=10 mm).

6.4 Mechanical properties of cylindrical NS structure with true NS filler

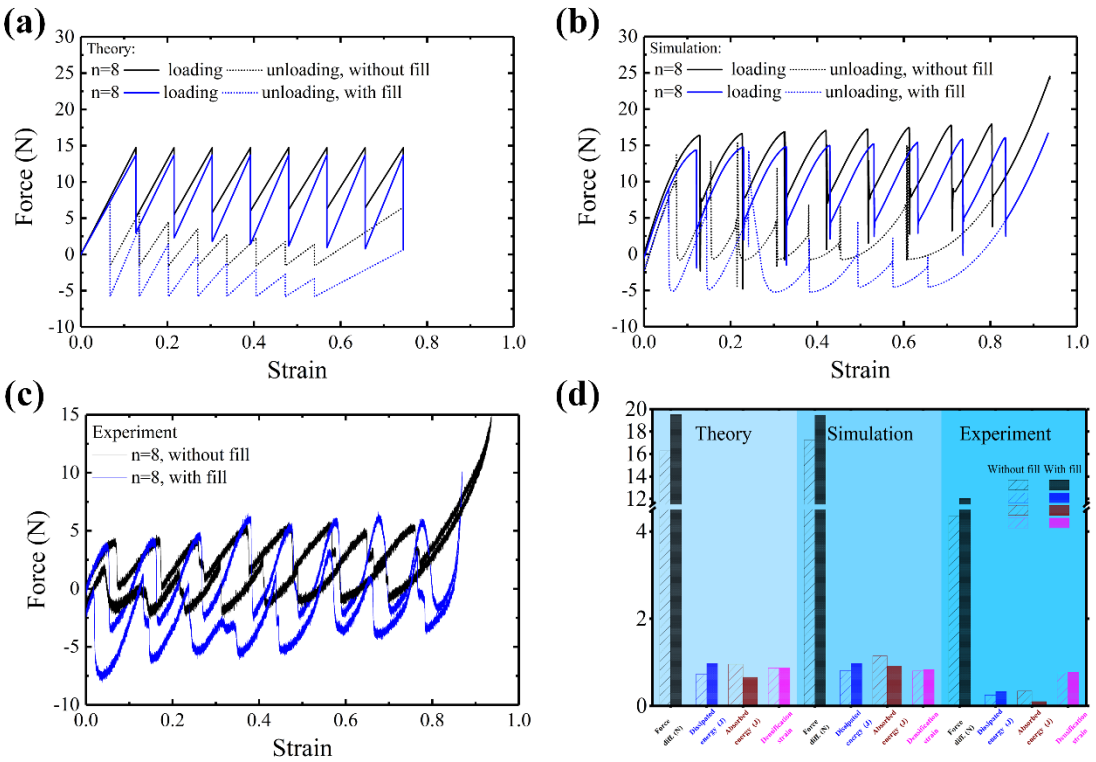

Fig. 25. Comparison of loading-unloading response from: (a) theory; (b) simulation; and (c) experiment, for unfilled and filled cylindrical NS structure with true NS filler (magnets systems). (-k_2/2). (d) Comparison of each property for unfilled and filled cylindrical NS structure.

In addition to the above methods, one other strategy, decreasing the peak and the minimum force simultaneously, and ensuring the variation magnitude of the peak force smaller than that of the minimum force, is also worth trying to improve the cylindrical NS structure's energy dissipation capacity. In general, the filler is usually used to improve the mechanical properties and it is hard to decrease the peak and the minimum force simultaneously. Using reverse thinking, if the structure is filled with the negative stiffness filler, the aim, decreasing the peak and the minimum force simultaneously can be realized. Here, the magnets system, exhibiting true negative stiffness, is introduced to demonstrate the effect of the strategy experimentally.

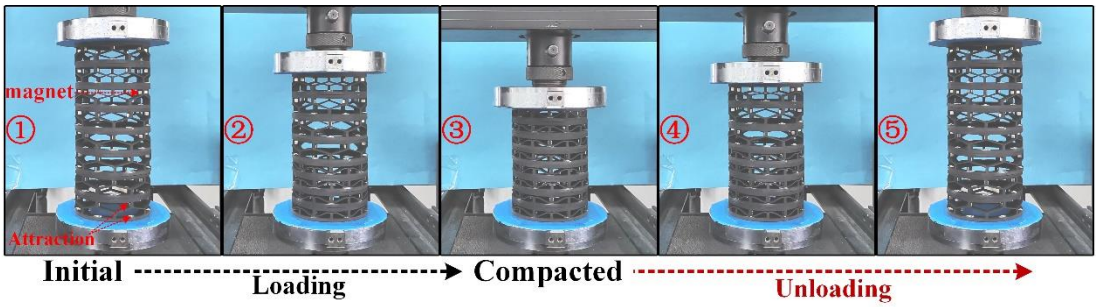

Fig. 26. Deformation processes from experiments for filled cylindrical NS structure with true NS filler (magnets systems) when under loading-unloading test. (n=8)

The mechanical properties of the filled cylindrical NS structure with true negative stiffness filler are first investigated through the simulations and the theory. The true negative stiffness filler is replaced by a negative stiffness spring in the FE model, in which the stiffness of the spring is set as $\frac{k_2}{2}$. The loading-unloading response curves

of the cylindrical NS structure with true negatives stiffness filler from theory and simulation are presented in Fig. 25(a) and (b). The theoretical and simulation results are in good agreement with each other, suggesting that the theory can well describe the mechanical characteristics of the filled cylindrical NS structure and has high precision. Moreover, the theoretical and simulation results both show that the peak force in the loading path and the minimum force in the unloading path decrease together with the influence of the filler. The decrease in the peak force is far smaller than the decrease in the minimum force, and this change is conductive to expand the enclosed area between the loading and unloading response curves.

The influence of the true NS filler on the mechanical properties of the cylindrical NS structure is also demonstrated by the experiments. The magnets system is selected to act as the true NS filler, and the rationality of the selection has been explained in Section 3. The whole deformation processes of the filled cylindrical NS structure under the loading-unloading test are displayed in Fig. 26. The experimental response curves of the unfilled and the filled cylindrical NS structure are shown in Fig. 25(c). The enclosed area between the response curves of the filled cylindrical NS structure is obviously larger than that of the unfilled one, and the dissipation energy increases by 40% due to the effect of the embedded magnets system.

The force difference, dissipated energy, absorbed energy, and the densification strain of the unfilled and the filled cylindrical NS structure are figured out and presented in Fig. 25(d). The force difference obtained from different method all increases with the effect of the filler, which directly contributes to the improvement of the energy

dissipation. The energy absorption decreases due to the decrease of the force plateau. The change of the densification strain is tiny and can almost be neglected. The property variation trends from the different methods are consistent, while there is a minor error on the changing magnitude between the experiment and the other methods. The cause of the error for the unfilled cylindrical NS structure has been demonstrated in the above content. The magnet filler, employed as the negative stiffness here, is of nonlinear stiffness, as shown in Fig. 7(d), and its stiffness is not entirely the same as the setting in theory and simulation. At present, there is no perfect linear elastic filler with negative stiffness. Thus, the magnets were applied to demonstrate the effect of the presented method. Overall, the error is the result of the combined effect of multiple factors.

Based on the above results, it can be concluded that harnessing the true NS filler can really enhance the energy dissipation capacity of the cylindrical NS structure. The magnets systems do not dissipate energy during the loading-and-unloading test. The increment of the cylindrical NS structure's dissipation energy is owing to the effect of the true NS filler on the snap-through and snap-back behavior.

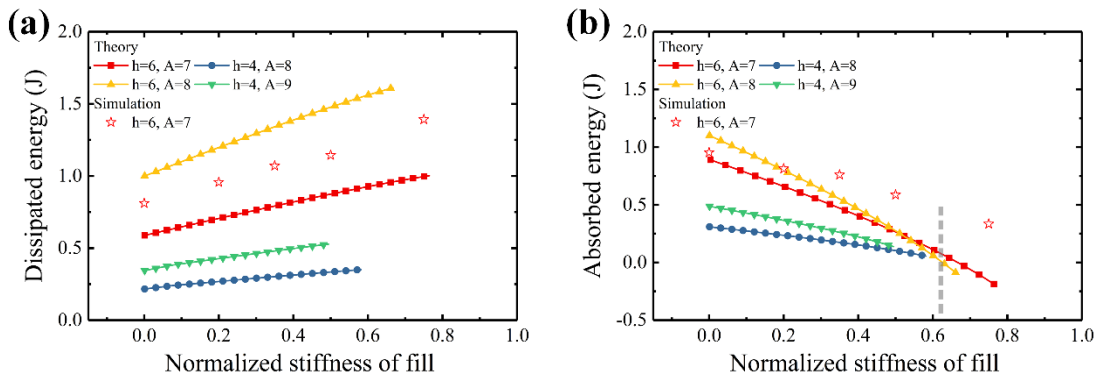

Fig. 27. Relationship between filler's stiffness and: (a) energy dissipation capacity; (b) energy absorption capacity.

The changing laws of the energy dissipation and the energy absorption with the increment of the filler's stiffness are studied, and the results are presented in Fig. 27. The normalized stiffness of the filler can be expressed as $\left|\frac{k_{filler}}{k_2}\right|$. The energy dissipation would linearly grow, while the energy absorption would gradually decrease with the increment of the filler's normalized stiffness. The simulation results exhibit the same changing trend as the theory, which further proves the theory. The energy absorption would decrease and even become negative (on the right part of the grey dotted line) as the filler's stiffness increases, which indicated the response force during the loading path may be entirely negative. Negative response force during loading path is not reasonable and will not happen in reality. The theory here neglects the filler's influence on the structure's initial states. If the attraction force between the magnets is big enough, the cylindrical structure would deform immediately once filling the magnets. Therefore, when applying this improved strategy, the absolute value of the filler's stiffness should be far less than the k_1 of the cylindrical NS structures.

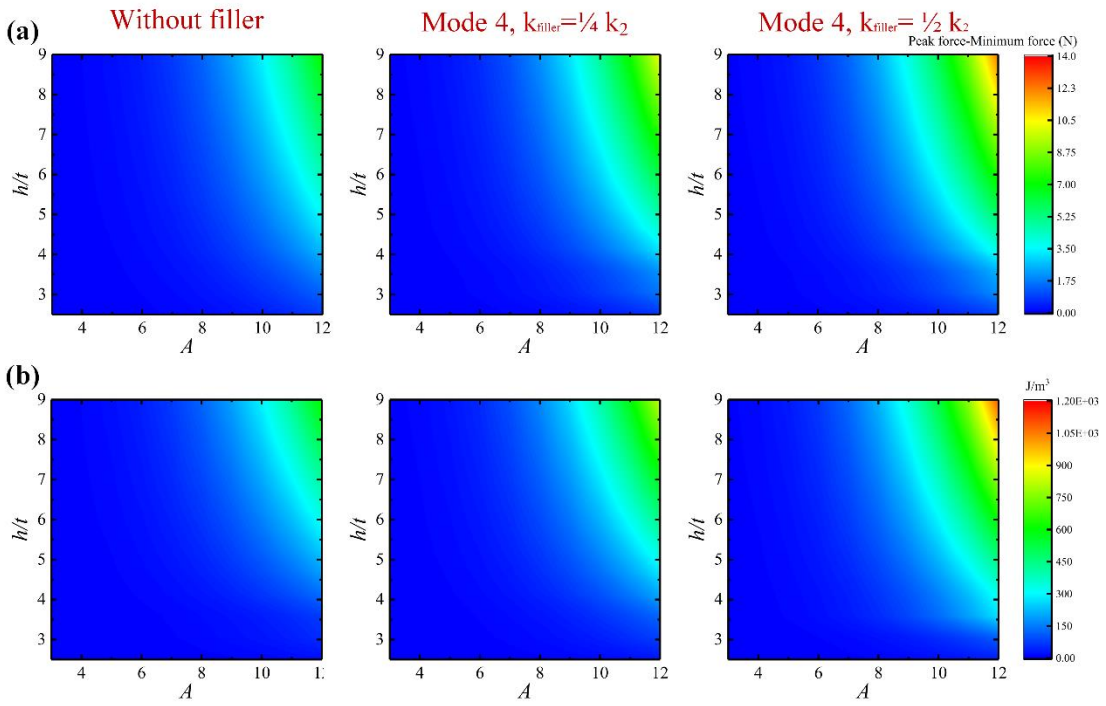

Fig. 28. Comparison of: (a) force difference; (b) specific energy dissipation for unfilled and filled cylindrical NS structures ($k_{filler}=k_2/4$ and $k_{filler}=k_2/2$). (n=16, R=40 mm, b=10 mm).

The influence of the structural parameters on the force difference and the specific energy dissipation of the cylindrical NS structure is investigated through the theory, and the results are presented in Fig. 28. The relationships between the parameters (h/t and A) and the properties for the filled cylindrical NS structure are consistent with those for the unfilled cylindrical ones. The force difference and the specific energy dissipation would increase with the parameters, h/t, and A. Moreover, there is a remarkable rise in the dissipation energy of the filled structure as the stiffness of the filler decreases from $\frac{k_2}{4}$ to $\frac{k_2}{2}$ $(k_2 < 0)$.

Although the strategy, introducing the true NS filler, is effective in improving the energy dissipation capacity, it would weaken the load-bearing capacity of the cylindrical NS structure and the energy absorption capacity. Therefore, striking a

balance between the energy dissipation capacity and other properties based on application scenarios is critical.

7. Conclusion

This study sets out to optimize the mechanical properties of the cylindrical NS structure via introducing filler and investigate the detailed effects of the filler types on the structure's mechanical properties. Theoretical models for describing the mechanical responses of the local NS element, the unfilled and the filled cylindrical NS structure are all presented in this study. With a combination of the experiment, the simulation, and the presented theory, the basic mechanical properties, the energy dissipation and absorption capacity of the unfilled and the filled cylindrical NS structure with different filler types (the linear elastic filler, the visco-hyperelastic filler, and the true NS filler) are systematically investigated and discussed. The research results suggest that the linear elastic filler would weaken the cylindrical NS structure's energy dissipation capacity but can improve its energy absorption. The visco-hyperelastic filler can effectively improve the strength, energy dissipation, and absorption capacity, provided the equivalent stiffness of the filler is well matched with those of the cylindrical NS structure. One of the interesting findings from this study is that the cylindrical NS structure with true NS filler can possess lower strength and better energy dissipation capacity simultaneously than the unfilled one.

This work comprehensively investigated the filled NS structure (mechanical metamaterials) and provided new insight into the influence of the filler types on the mechanical properties of the filled cylindrical NS structures. The presented theory for

characterizing the filled and the unfilled cylindrical NS structures' mechanical response is of universality and lays the groundwork for future research into other filled NS mechanical metamaterials. In addition, a novel strategy, harnessing the true NS filler to improve the cylindrical NS structure's energy dissipation capacity, is first proposed and verified in this study. This strategy is worth trying in the optimization of other energy-absorption materials.

The research in this paper is original, and the obtained conclusions are of some reference value. However, some limits do exist in this study. The major limitation of this study is that the precision of the theoretical model for describing the mechanical responses of the structure's local element is not very high. Moreover, the influence of the strain rates on the mechanical properties of the cylindrical NS structure with visco-hyperelastic filler lacks research. In order to overcome the above limits, the theory with high precision for the NS, spatial inclined beam elements is worth studying. Additionally, dynamic tests can be employed to compare the mechanical properties of filled and unfilled cylindrical NS structures in future work.

Acknowledgments

The present work is supported by National Natural Science Foundation of China under Grant No. 11972008, Natural Science Foundation of Heilongjiang Province under Grant No. A2018005, and Innovation Project of New Energy Vehicle and Intelligent Connected Vehicle.

Reference

1 Meaud, J. & Che, K. Tuning elastic wave propagation in multistable architected materials. *International Journal of Solids and Structures* **122-123**, 69-80,

doi:10.1016/j.ijsolstr.2017.05.042 (2017).

2 Nadkarni, N., Arrieta, A. F., Chong, C., Kochmann, D. M. & Daraio, C. Unidirectional Transition Waves in Bistable Lattices. *Phys Rev Lett* **116**, 244501, doi:10.1103/PhysRevLett.116.244501 (2016).

3 Raney, J. R. *et al.* Stable propagation of mechanical signals in soft media using stored elastic energy. *Proceedings of the National Academy of Sciences of the United States of America* **113**, 9722 (2016).

4 Jang, J. H., Koh, C. Y., Bertoldi, K., Boyce, M. C. & Thomas, E. L. Combining pattern instability and shape-memory hysteresis for phononic switching. *Nano Letters* **9**, 2113-2119 (2009).

5 Holmes, D. P. & Crosby, A. J. Snapping surfaces. *Advanced Materials* **19**, 3589-3593, doi:10.1002/adma.200700584 (2007).

6 Li, J. *et al.* Switching periodic membranes via pattern transformation and shape memory effect. *Soft Matter* **8**, 10322-10328 (2012).

7 Le, T. D. & Ahn, K. K. Experimental investigation of a vibration isolation system using negative stiffness structure. *International Journal of Mechanical Sciences* **70**, 99-112 (2013).

8 Qiu, J., Lang, J. H. & Slocum, A. H. A curved-beam bistable mechanism. *Journal of Microelectromechanical Systems* **13**, 137-146 (2004).

9 Fulcher, B. A., Shahan, D. W., Haberman, M. R., Seepersad, C. C. & Wilson, P. S. Analytical and Experimental Investigation of Buckled Beams as Negative Stiffness Elements for Passive Vibration and Shock Isolation Systems. *Journal of Vibration & Acoustics* **136**, 031009 (2015).

10 Dai, F., Li, H. & Du, S. Design and analysis of a tri-stable structure based on bi-stable laminates. *Composites Part A: Applied Science and Manufacturing* **43**, 1497-1504, doi:10.1016/j.compositesa.2012.03.018 (2012).

11 Gomez, M., Moulton, D. E. & Vella, D. Dynamics of viscoelastic snap-through. *Journal of the Mechanics and Physics of Solids* **124**, 781-813, doi:10.1016/j.jmps.2018.11.020 (2019).

12 Yan, D., Pezzulla, M. & Reis, P. M. Buckling of pressurized spherical shells containing a through-thickness defect. *Journal of the Mechanics and Physics of Solids* **138**, 103923, doi:10.1016/j.jmps.2020.103923 (2020).

13 Sobota, P. M. & Seffen, K. A. Effects of boundary conditions on bistable behaviour in axisymmetrical shallow shells. *Proceedings. Mathematical, physical, and engineering sciences* **473**, 20170230, doi:10.1098/rspa.2017.0230 (2017).

14 Taffetani, M., Jiang, X., Holmes, D. P. & Vella, D. Static bistability of spherical caps. *Proceedings. Mathematical, physical, and engineering sciences* **474**, 20170910, doi:10.1098/rspa.2017.0910 (2018).

15 Filipov, E. T. & Redoutey, M. Mechanical characteristics of the bistable origami hypar. *Extreme Mechanics Letters* **25**, 16-26, doi:10.1016/j.eml.2018.10.001 (2018).

16 Yang, Y., Dias, M. A. & Holmes, D. P. Multistable kirigami for tunable architected materials. *Phys Rev Mater* **2**, doi:ARTN 11060110.1103/PhysRevMaterials.2.110601 (2018).

17 Hafez, M., Lichter, M. D. & Dubowsky, S. in *IEEE International Conference on Robotics and Automation, 2002. Proceedings. ICRA.* 335-340 vol.331.

18 Liu, X., Huang, X. & Hua, H. On the characteristics of a quasi-zero stiffness isolator using Euler buckled beam as negative stiffness corrector. *Journal of Sound & Vibration* **332**, 3359-3376 (2013).

19 Lee, C. M., Goverdovskiy, V. N. & Temnikov, A. I. Design of springs with “negative” stiffness to

improve vehicle driver vibration isolation. *Journal of Sound & Vibration* **302**, 865-874 (2007).

20 Huang, X., Liu, X., Sun, J., Zhang, Z. & Hua, H. Vibration isolation characteristics of a nonlinear isolator using Euler buckled beam as negative stiffness corrector: A theoretical and experimental study. *Journal of Sound & Vibration* **333**, 1132-1148 (2014).

21 Ando, B., Baglio, S., L'Episcopo, G. & Trigona, C. Investigation on Mechanically Bistable MEMS Devices for Energy Harvesting From Vibrations. *Journal of Microelectromechanical Systems* **21**, 779-790 (2012).

22 Brake, M. R. *et al.* Modeling and Measurement of a Bistable Beam in a Microelectromechanical System. *Journal of Microelectromechanical Systems* **19**, 1503-1514 (2010).

23 Saif, M. T. A. On a tunable bistable MEMS-theory and experiment. *Journal of Microelectromechanical Systems* **9**, 157-170 (2002).

24 Dong, L. & Lakes, R. Advanced damper with high stiffness and high hysteresis damping based on negative structural stiffness. *International Journal of Solids and Structures* **50**, 2416-2423, doi:10.1016/j.ijsolstr.2013.03.018 (2013).

25 Karpov, E. G., Ozevin, D., Mahamid, M. & Danso, L. A. On the comprehensive stability analysis of axially loaded bistable and tristable metastructures. *International Journal of Solids and Structures* **199**, 158-168, doi:10.1016/j.ijsolstr.2020.04.032 (2020).

26 Haghpanah, B., Shirazi, A., Salari-Sharif, L., Guell Izard, A. & Valdevit, L. Elastic architected materials with extreme damping capacity. *Extreme Mechanics Letters* **17**, 56-61, doi:10.1016/j.eml.2017.09.014 (2017).

27 Gorissen, B., Melancon, D., Vasios, N., Torbati, M. & Bertoldi, K. Inflatable soft jumper inspired by shell snapping. *Science Robotics* **5**, doi:ARTN eabb196710.1126/scirobotics.abb1967 (2020).

28 Tang, Y. *et al.* Leveraging elastic instabilities for amplified performance: Spine-inspired high-speed and high-force soft robots. *Science advances* **6**, eaaz6912, doi:10.1126/sciadv.aaz6912 (2020).

29 Harne, R. L. & Wang, K. W. A review of the recent research on vibration energy harvesting via bistable systems. *Smart Materials & Structures* **22**, 023001 (2013).

30 Kuder, I. K., Arrieta, A. F., Raither, W. E. & Ermanni, P. Variable stiffness material and structural concepts for morphing applications. *Progress in Aerospace Sciences* **63**, 33-55 (2013).

31 Prasad, J. & Diaz, A. R. Synthesis of Bistable Periodic Structures Using Topology Optimization and a Genetic Algorithm. *Journal of Mechanical Design* **128**, 1298, doi:10.1115/1.2338576 (2006).

32 Feeny, B. F. & Diaz, A. R. Twinkling Phenomena in Snap-Through Oscillators. *Journal of Vibration and Acoustics* **132**, 061013, doi:10.1115/1.4000764 (2010).

33 Benichou, I. & Givli, S. Structures undergoing discrete phase transformation. *Journal of the Mechanics & Physics of Solids* **61**, 94-113 (2013).

34 Findeisen, C., Hohe, J., Kadic, M. & Gumbsch, P. Characteristics of mechanical metamaterials based on buckling elements. *Journal of the Mechanics & Physics of Solids* **102** (2017).

35 Misra, A., Raney, J. R., De Nardo, L., Craig, A. E. & Daraio, C. Synthesis and characterization of carbon nanotube-polymer multilayer structures. *ACS Nano* **5**, 7713-7721, doi:10.1021/nn202262j (2011).

36 Raney, J. R., Misra, A. & Daraio, C. Tailoring the microstructure and mechanical properties of arrays of aligned multiwall carbon nanotubes by utilizing different hydrogen concentrations during synthesis. *Carbon* **49**, 3631-3638, doi:10.1016/j.carbon.2011.04.066 (2011).

37 Raney, J. R., Fraternali, F., Amendola, A. & Daraio, C. Modeling and in situ identification of material parameters for layered structures based on carbon nanotube arrays. *Composite Structures* **93**, 3013-3018, doi:10.1016/j.compstruct.2011.04.034 (2011).

38 Misra, A., Raney, J. R., Craig, A. E. & Daraio, C. Effect of density variation and non-covalent functionalization on the compressive behavior of carbon nanotube arrays. *Nanotechnology* **22**, 425705, doi:10.1088/0957-4484/22/42/425705 (2011).

39 Restrepo, D., Mankame, N. D. & Zavattieri, P. D. Phase transforming cellular materials. *Extreme Mechanics Letters* **4**, 52-60 (2015).

40 Florijn, B., Coulais, C. & van Hecke, M. Programmable mechanical metamaterials. *Phys Rev Lett* **113**, 175503, doi:10.1103/PhysRevLett.113.175503 (2014).

41 Correa, D. M. *et al.* Negative stiffness honeycombs for recoverable shock isolation. *Rapid Prototyping Journal* **21**, 193-200 (2015).

42 Chan, S. H., Lakes, R. S. & Plesha, M. E. Design, Fabrication, and Analysis of Lattice Exhibiting Energy Absorption via Snap-through Behavior. *Materials & Design* (2018).

43 Ha, C. S., Lakes, R. S. & Plesha, M. E. Cubic negative stiffness lattice structure for energy absorption: Numerical and experimental studies. *International Journal of Solids and Structures* **178-179**, 127-135, doi:10.1016/j.ijsolstr.2019.06.024 (2019).

44 Zhang, Y., Restrepo, D., Velay-Lizancos, M., Mankame, N. D. & Zavattieri, P. D. Energy dissipation in functionally two-dimensional phase transforming cellular materials. *Sci Rep* **9**, 12581, doi:10.1038/s41598-019-48581-8 (2019).

45 Frenzel, T., Findeisen, C., Kadic, M., Gumbsch, P. & Wegener, M. Tailored Buckling Microlattices as Reusable Light-Weight Shock Absorbers. *Advanced Materials* **28**, 5865-5870 (2016).

46 Haghpanah, B., Salari‐Sharif, L., Pourrajab, P., Hopkins, J. & Valdevit, L. Multistable Shape‐Reconfigurable Architected Materials. *Advanced Materials* **28**, 7915-7920 (2016).

47 Alturki, M. & Burgueño, R. Multistable Cosine-Curved Dome System for Elastic Energy Dissipation. *Journal of Applied Mechanics* **86**, 091002, doi:10.1115/1.4043792 (2019).

48 Pan, F. *et al.* 3D Pixel Mechanical Metamaterials. *Adv Mater*, e1900548, doi:10.1002/adma.201900548 (2019).

49 Liu, S., Azad, A. I. & Burgueño, R. Architected materials for tailorable shear behavior with energy dissipation. *Extreme Mechanics Letters* **28**, 1-7, doi:10.1016/j.eml.2019.01.010 (2019).

50 Tan, X. *et al.* Novel multi-stable mechanical metamaterials for trapping energy through shear deformation. *International Journal of Mechanical Sciences* **164**, 105168, doi:10.1016/j.ijmecsci.2019.105168 (2019).

51 Tan, X. *et al.* Mechanical response of negative stiffness truncated-conical shell systems: experiment, numerical simulation and empirical model. *Composites Part B: Engineering* **188**, 107898, doi:10.1016/j.compositesb.2020.107898 (2020).

52 Tan, X. *et al.* Real-time tunable negative stiffness mechanical metamaterial. *Extreme Mechanics Letters* **41**, 100990, doi:10.1016/j.eml.2020.100990 (2020).

53 Rafsanjani, A., Akbarzadeh, A. & Pasini, D. Snapping Mechanical Metamaterials under Tension. *Advanced Materials* **27**, 5931 (2015).

54 Hewage, T. A., Alderson, K. L., Alderson, A. & Scarpa, F. Double-Negative Mechanical Metamaterials Displaying Simultaneous Negative Stiffness and Negative Poisson's Ratio Properties. *Advanced Materials* **28** (2016).

55 Rafsanjani, A. & Pasini, D. Bistable auxetic mechanical metamaterials inspired by ancient

geometric motifs. *Extreme Mechanics Letters* **9**, 291-296 (2016).

56 Chen, T., Mueller, J. & Shea, K. Integrated Design and Simulation of Tunable, Multi-State Structures Fabricated Monolithically with Multi-Material 3D Printing. *Scientific Reports* **7**, 45671 (2017).

57 Zhang, Y., Wang, Q., Tichem, M. & van Keulen, F. Design and characterization of multi-stable mechanical metastructures with level and tilted stable configurations. *Extreme Mechanics Letters*, 100593, doi:10.1016/j.eml.2019.100593 (2019).

58 Bobbert, F. S. L., Janbaz, S., van Manen, T., Li, Y. & Zadpoor, A. A. Russian doll deployable meta-implants: Fusion of kirigami, origami, and multi-stability. *Materials & Design* **191**, 108624, doi:10.1016/j.matdes.2020.108624 (2020).

59 Katz, S. & Givli, S. Solitary waves in a bistable lattice. *Extreme Mechanics Letters* (2018).

60 Tan, X. *et al.* Programmable Buckling-based negative stiffness metamaterial. *Materials Letters*, 127072, doi:10.1016/j.matlet.2019.127072 (2019).

61 Meaud, J. Multistable two-dimensional spring-mass lattices with tunable band gaps and wave directionality. *Journal of Sound and Vibration* **434**, 44-62, doi:10.1016/j.jsv.2018.07.032 (2018).

62 Morris, C., Bekker, L., Spadaccini, C., Haberman, M. & Seepersad, C. Tunable Mechanical Metamaterial with Constrained Negative Stiffness for Improved Quasi‐Static and Dynamic Energy Dissipation. *Advanced Engineering Materials*, 1900163, doi:10.1002/adem.201900163 (2019).

63 Shan, S. *et al.* Multistable Architected Materials for Trapping Elastic Strain Energy. *Advanced Materials* **27**, 4296-4301 (2015).

64 Debeau, D. A., Seepersad, C. C. & Haberman, M. R. Impact behavior of negative stiffness honeycomb materials. *Journal of Materials Research* **33**, 290-299 (2018).

65 Tan, X. J., Wang, B., Chen, S., Zhu, S. W. & Sun, Y. G. A novel cylindrical negative stiffness structure for shock isolation. *Composite Structures* **214**, 397-405, doi:10.1016/j.compstruct.2019.02.030 (2019).

66 Chen, S. *et al.* A novel composite negative stiffness structure for recoverable trapping energy. *Composites Part A: Applied Science and Manufacturing* **129**, 105697, doi:10.1016/j.compositesa.2019.105697 (2020).

67 Tan, X. J. *et al.* Design, fabrication, and characterization of multistable mechanical metamaterials for trapping energy. *Extreme Mechanics Letters* **28**, 8-21, doi:10.1016/j.eml.2019.02.002 (2019).

68 Tan, X. *et al.* Novel multidirectional negative stiffness mechanical metamaterials. *Smart Materials and Structures* **29**, 015037, doi:10.1088/1361-665X/ab47d9 (2020).

69 Bertoldi, K. Harnessing Instabilities to Design Tunable Architected Cellular Materials. *Annual Review of Materials Research* **47** (2017).

70 Shang, X., Liu, L., Rafsanjani, A. & Pasini, D. Durable bistable auxetics made of rigid solids. *Journal of Materials Research* **33**, 300-308, doi:10.1557/jmr.2017.417 (2017).

71 Fu, K., Zhao, Z. & Jin, L. Programmable Granular Metamaterials for Reusable Energy Absorption. *Advanced Functional Materials*, 1901258, doi:10.1002/adfm.201901258 (2019).

72 Cortes, S. *et al.* Design, Manufacture, and Quasi-Static Testing of Metallic Negative Stiffness Structures within a Polymer Matrix. *Experimental Mechanics* **57**, 1-9 (2017).

73 Deng, H., Cheng, L., Liang, X., Hayduke, D. & To, A. C. Topology optimization for energy dissipation design of lattice structures through snap-through behavior. *Computer Methods in*

Applied Mechanics and Engineering **358**, 112641, doi:10.1016/j.cma.2019.112641 (2020).

74 Zhu, S. *et al.* Bio-inspired multistable metamaterials with reusable large deformation and ultra-high mechanical performance. *Extreme Mechanics Letters* **32**, 100548, doi:10.1016/j.eml.2019.100548 (2019).

75 Milton, G. W. The Theory of Composites *Cambridge: Cambridge University Press*, doi:10.1017/CBO9780511613357 (2002).

76 Wang, B. *et al.* Cushion performance of cylindrical negative stiffness structures: Analysis and optimization. *Composite Structures* **227**, 111276, doi:10.1016/j.compstruct.2019.111276 (2019).

77 Zhu, S. *et al.* Quasi‐All‐Directional Negative Stiffness Metamaterials Based on Negative Rotation Stiffness Elements. *physica status solidi (b)*, 1900538, doi:10.1002/pssb.201900538 (2020).

78 Brinkmeyer, A., Santer, M., Pirrera, A. & Weaver, P. M. Pseudo-bistable self-actuated domes for morphing applications. *International Journal of Solids & Structures* **49**, 1077-1087 (2012).

79 Hua, J., Lei, H., Zhang, Z., Gao, C. & Fang, D. Multistable Cylindrical Mechanical Metastructures: Theoretical and Experimental Studies. *Journal of Applied Mechanics* **86**, doi:10.1115/1.4043283 (2019).

80 Younis, M. I. & Hussein, H. Analytical Study of the Snap-Through and Bistability of Beams With Arbitrarily Initial Shape. *Journal of Mechanisms and Robotics* **12**, doi:10.1115/1.4045844 (2020).

81 Ju, M. L., Mezghani, S., Jmal, H., Dupuis, R. & Aubry, E. Parameter Estimation of a Hyperelastic Constitutive Model for the Description of Polyurethane Foam in Large Deformation. *Cell Polym* **32**, 21-40, doi:Doi 10.1177/026248931303200102 (2013).

82 Ju, M. L., Jmal, H., Dupuis, R. & Aubry, E. Visco-hyperelastic constitutive model for modeling the quasi-static behavior of polyurethane foam in large deformation. *Polymer Engineering & Science* **55**, 1795-1804, doi:10.1002/pen.24018 (2015).

83 Xu, P. *et al.* The investigation of viscoelastic mechanical behaviors of bolted GLARE joints: Modeling and experiments. *International Journal of Mechanical Sciences* **175**, 105538, doi:10.1016/j.ijmecsci.2020.105538 (2020).